CHEMICAL REVIEWS

Review

pubs.acs.org/CR

Disease Detection and Management via Single Nanopore-Based Sensors

Joseph E. Reiner,*[,†] Arvind Balijepalli,[‡,§] Joseph W. F. Robertson,[‡] Jason Campbell,[‡] John Suehle,[‡] and John J. Kasianowicz[‡]

[†]Department of Physics, Virginia Commonwealth University, 701 W. Grace Street, Richmond, Virginia 23284, United States

[‡]Physical Measurement Laboratory, National Institute of Standards and Technology, Gaithersburg, Maryland 20899-8120, United States

[§]Laboratory of Computational Biology, National Heart Lung and Blood Institute, Rockville, Maryland 20852, United States

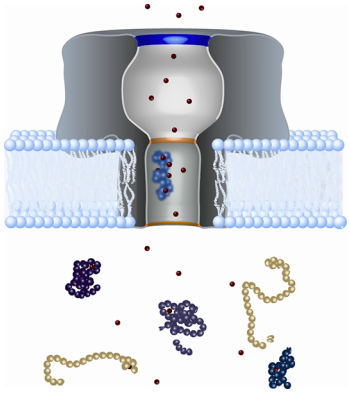

CONTENTS

1. INTRODUCTION

1.1. Channels and Porins: Current and Possible Future Roles

As nanometer-scale portals in biological membranes, protein ionic channels act as gatekeepers, controlling the traffic of ions and macromolecules into and out of cells, organelles, and the nucleus. Because of their ubiquitous nature, proper channel function is critical to all aspects of life. One might suppose that the most obvious feature of these transmembrane proteins, a nanometer-scale hole in a ca. 4 nm thick phospholipid bilayer membrane,[1,2] renders channels as the simplest of biological machines. However, channels have evolved in rather sophisticated ways to control a wide range of biological function. We briefly discuss below some of the roles channels play in biology, as well as why they and mimics of them are emerging as effective biosensors for characterizing and quantifying many types of molecules. We then describe some examples of how such a novel measurement capability could prove useful for detecting disease states, assessing the efficacy of therapeutic agents, and managing the treatment of human disease.

Special Issue: 2012 Ion Channels and Disease

Received: September 13, 2012
Published: November 16, 2012

1.2. Seemingly Simple Structures, But Ubiquitous in Function

Channels are perhaps most well-known because they are the molecular basis of nerve and muscle activity.[3] They also aid in trafficking of nucleic acids and proteins across the nuclear membrane,[4−6] proteins into and across cell walls,[7−11] and water across a wide range of membranes.[12,13] Channels have also evolved to sustain and promote life, including limiting the cellular life cycle (apoptosis and programmed cell death), and dysfunction in these channels can result in diseases such as cancer.[14−17] As if it was a cruel twist of fate, properly functioning ion channels can also directly cause disease and death, as some bacteria secrete pore-forming toxins that either make membranes indiscriminately leaky to ions (thereby dissipating concentration and/or electrostatic potential gradients) or transport other toxins into cells.[18−23]

1.3. Ion Transport Regulation: Gating and Chemical Specificity

In nerve, channels that control the transport of Na^+ and K^+ ions[3,24−32] cause an electrical signal, the action potential, to propagate at <1 m/s along axons (Figure 1, left). At the nexus

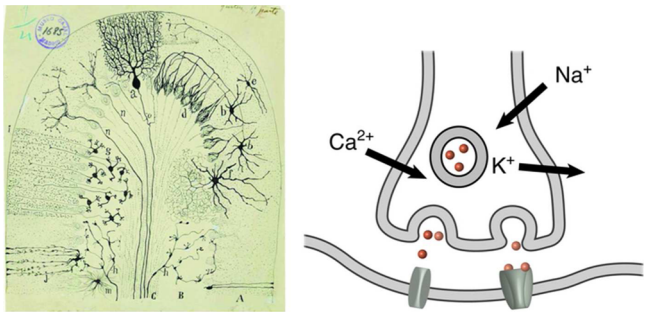

Figure 1. Signal transmission in nerve. Long-distance signal transmission in nerve fibers is propagated along axons. One of many classical drawings of the neural network in the cerebellar cortex by Santiago Ramon y Cajal visualized with the aid of Golgi stains (left). Reproduced with permission from ref 271. Copyright 2003 Nature Publishing Group. These signals, action potentials, are caused by the spatial and temporal change in membrane permeability to Na^+ and K^+ ions along the length of an axon. At the synapse (the junction between two neurons), the action potential causes an influx of Ca^{2+} ions and the subsequent release of neurotransmitters stored in vesicles into the synaptic cleft (right). The binding of neurotransmitters to receptor channels in the postsynaptic neuron causes the channels to open, which initiates an action potential in that cell, and continues the signal propagation to either the brain or muscle. This class of channels acts as a highly specific and sensitive single-molecule chemical detector.

between two neurons (Figure 1, right), the action potential opens Ca^{2+}-specific channels, and the influx of the divalent cations induces neurotransmitter-laden vesicles to release their cargo into the 20-nm wide synaptic cleft. The binding of neurotransmitters to receptor channels in the postsynaptic nerve membrane (or muscle end plate) modulates the spontaneous gating in these channels between different conducting states (Figure 1, left). The lesson to be learned here is that some channels are designed to detect the presence of specific chemicals.

Interestingly, the chemical selectivity of receptor channels is not perfect, and some small molecules can bind to nonreceptor channels. For example, acetylcholine and the nonapeptide oxytocin[33] (Figure 2, left) are neurotransmitters and bind to

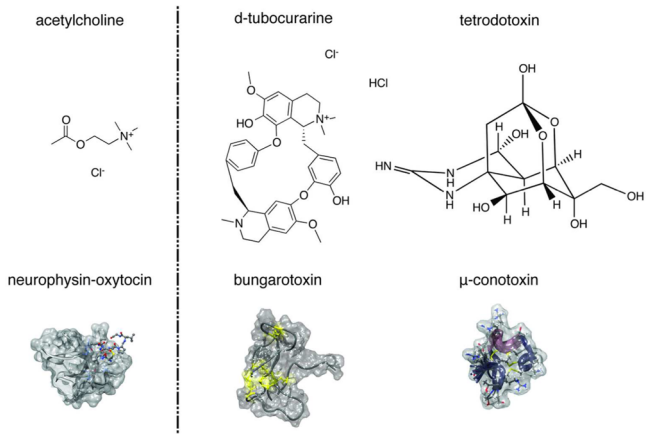

Figure 2. Neutrotransmitters and other small molecules modulate ion channels. These include range from acetylcholine to neurophysin-oxytocin (left). Interestingly, channel function can be confounded by toxins produced by plants and animals (e.g., *d*-tubocurarine, tetrodotoxin, bugarotoxin, and *μ*-conotoxin; right).

their respective channels. However, other channels can bind toxins from snake venom (e.g., *Bungarus multicinctus*),[34] puffer fish organs (*tetrodotoxin*, which is produced by a symbiotic bacteria), jellyfish (*saxitoxin*), plants (*curare*), and snails (conotoxins[35]) (Figure 2, right). Despite the obvious health issues caused by these and other toxins, there is an upside to their action. For example, the ability to alter channel activity with small molecules is emerging as an aid to the management of chronic pain.[36]

2. PRINCIPLES OF ION CHANNEL-BASED DETECTORS

2.1. Mimicking Channel Sensor Capability

Because of the ability of some channels to respond, with high specificity, to certain analytes, it might seem straightforward to use channels for the detection of biological molecules and other analytes. Conceptually, the binding of an analyte to the pore would cause the channel to change conformation and, thus, its conductance. However, that kind of biomimicry is not straightforward for several reasons. In some cases, the binding of analytes (e.g., neurotransmitters) to channels causes the latter to change their average conformation, a process that is difficult to rationally design and control. Also, many channels tend to spontaneously gate between different conducting states or gate in response to an applied potential due to either a change in the pore volume[37] or the movement of a charged gate in the pore.[38−40] These processes would obviously confound the detection of many analytes. Although not a general solution to gating artifacts for all channels, that problem was solved[41] for the channel formed by the bacterial exotoxin *Staphylococcus aureus* *α*-hemolysin,[42] which enabled its use for a wide range of academic biosensing applications.[43] Thus, the goal is to mimic the general principle of analyte detection by channels and refine it with a simpler measurement design.

The three-dimensional structure of the *α*-hemolysin channel was determined to a resolution of 0.19 nm.[44] Aksimentiev and Schulten used molecular dynamics (MD) simulations to study this channel in great detail.[45] The simulations were used to estimate the diameter of the pore and the permeability of water through its side channels. By applying an electric potential across the pore, they were able to reproduce the open-channel conductivity and calculate the electrostatic potential along the

dx.doi.org/10.1021/cr300381m | *Chem. Rev.* 2012, 112, 6431−6451

length of the pore. As we show below, the pore is ideally suited to detecting small macromolecules and probing their physical properties.

In addition to the ability to control its spontaneous and voltage-dependent gating[41] and interact with synthetic polymers,[46−49] RNA and DNA polynucleotides,[50−56] the channel's geometry makes the pore an ideal platform for channel-based sensor studies.[43] For example, the channel has a large, extramembraneous segment that contains a relatively large diameter vestibule, which facilitates the capture of macromolecules,[52,57] and a narrower stem region that just spans a lipid bilayer membrane.[44,58] The constriction between these two segments is a barrier for polymer translocation that can be overcome with a sufficiently large applied potential.[52,56,59] Since then, other channels (e.g., OmpF[60] and MspA[61]) have been used for macromolecular sensing and characterization and will be briefly discussed below.

2.2. Chemical Interactions Are Critical

The question at hand is whether a fully open nanopore can transduce the presence of an analyte into an intelligible signal. This may seem trivial at first glance. After all, if an analyte enters a channel, it will change the pore conductance by either a field effect or by volume exclusion (i.e., as a nanoscale resistive-pulse Coulter counter).[62−64] The complete description is not that simple,[65] and ignoring the nuances of these measurements limits the range of questions and methods that can be applied to analyze more complicated samples.

Even if a nanometer-scale pore remains fully open under a wide range of applied potentials and solution conditions, there are several issues that could limit its use as an analytical sensor. Unless the sample is highly enriched in the target analyte, the pore needs to be highly selective to find the "needle in a haystack". In addition, if the analyte in question is too large to enter the channel pore, or cannot alter the pore conductance by binding to the channel exterior, another method to detect it with the channel is needed. These two points are discussed later in this review.

Perhaps more fundamentally, we need to consider whether the signal caused by an analyte is sufficiently large to be measured accurately. Because ion channels are nanometer scale in length, the one-dimensional diffusion equation[66] suggests that a particle with diffusion coefficient D will migrate a mean distance λ_x in a time t according to

$$\lambda_x = \sqrt{2Dt} \tag{1}$$

Thus, a small analyte ($D \approx 10^{-5}$ cm^2 s^{-1}) will diffuse the length of a channel that spans a 4-nm-thick lipid bilayer membrane in $t \approx 10$ ns. For a channel with a fully open single-channel conductance of $g \approx 1$ nS, an applied potential of $V \approx 100$ mV will drive less than tens of ions past the analyte while it is in the pore. Thus, if an analyte migrates through the pore via diffusion (electrodiffusion), it cannot be detected in such a short time because of insufficient counting statistics (even if the system had sufficient bandwidth). Thus, the trick is to keep the analyte in the pore for much longer intervals. This is precisely what receptor channels do and what happens when toxins bind to other types of channels.

Single analyte molecules binding to the nanopore can be understood conceptually by appealing to the chemical binding model. Consider an analyte (A) and a channel (C) that bind reversibly according to a simple reaction scheme:

$$\mathrm{A} + \mathrm{C} \underset{k_{off}}{\overset{k_{on}}{\rightleftarrows}} \mathrm{A/C} \tag{2}$$

where A/C is the analyte/channel complex and k_{on} and k_{off} are the rate constants for the association and the dissociation of the analyte to and from the channel, respectively. The binding constant for the reaction, in units of molarity, is $K = k_{off}/k_{on}$. In the limit of low analyte concentration, the mean residence time of a single molecule in the pore is $\tau = 1/k_{off}$. For moderately strong binding, the analyte will spend considerable time in the pore. For example, for a binding constant $K \approx 1$ μM, $\tau \approx 1$ ms (assuming a diffusion-limited association constant, $k_{on} \approx 10^9$ M^{-1} s^{-1}). In that case, using the same values of single-channel conductance and applied potential described above, ca. 10^6 ions will flow past the analyte, a considerable improvement in counting statistics! The reaction can be purely chemical in nature, as suggested by eq 2, or due to other physical processes (e.g., friction[67] or intermolecular interactions[68]).

With this chemical reaction scheme in mind, Figure 3 illustrates the basic principles of detecting analytes with a channel. The interaction of a single analyte and the channel pore will cause relatively long-lived conductance changes (Figure 3, top). Here, we assume the analyte reduces the conductance (perhaps due to volume exclusion), but it is conceivable that a charged analyte might bind to the pore mouth and modulate the conductance up or down by a field effect. Increasing the analyte concentration will increase the

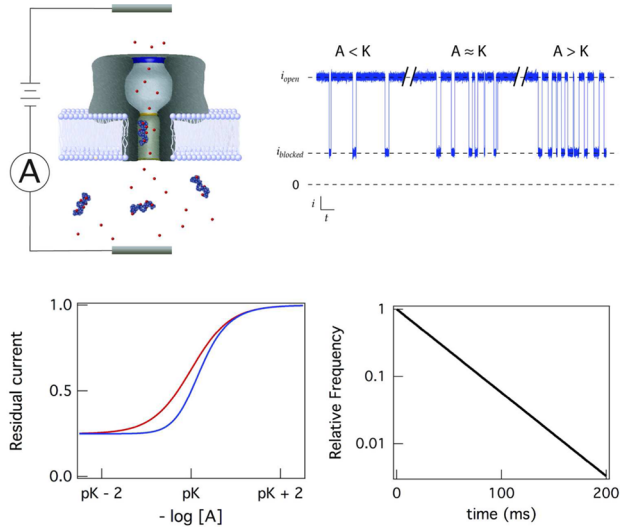

Figure 3. Principles of nanopore-based sensing. Individual molecules enter and exit the channel pore (top left) and cause transient ionic current blockades (top right). Increasing the analyte concentration, [A], relative to the binding constant, K, increases the rate these molecules partition into the pore and therefore the likelihood of detecting the species. For an ensemble of identical channels, the mean current is reduced with increasing analyte concentration until it matches the ratio of the current in a blocked single channel to that of a fully open channel (bottom left), assuming the pore reacts with one (red) or two (blue) analytes at a time. The residence-time distribution of analyte-induced current blockade depths provides information about the interactions between the analyte and the channel wall (bottom right). The degree of current blockade, residence-time distribution (a single exponential in this example, valid for the simplest chemical reaction model for the interactions between the analyte and the pore), and mean residence time can aid in the discrimination between different analytes.

dx.doi.org/10.1021/cr300381m | Chem. Rev. 2012, 112, 6431−6451

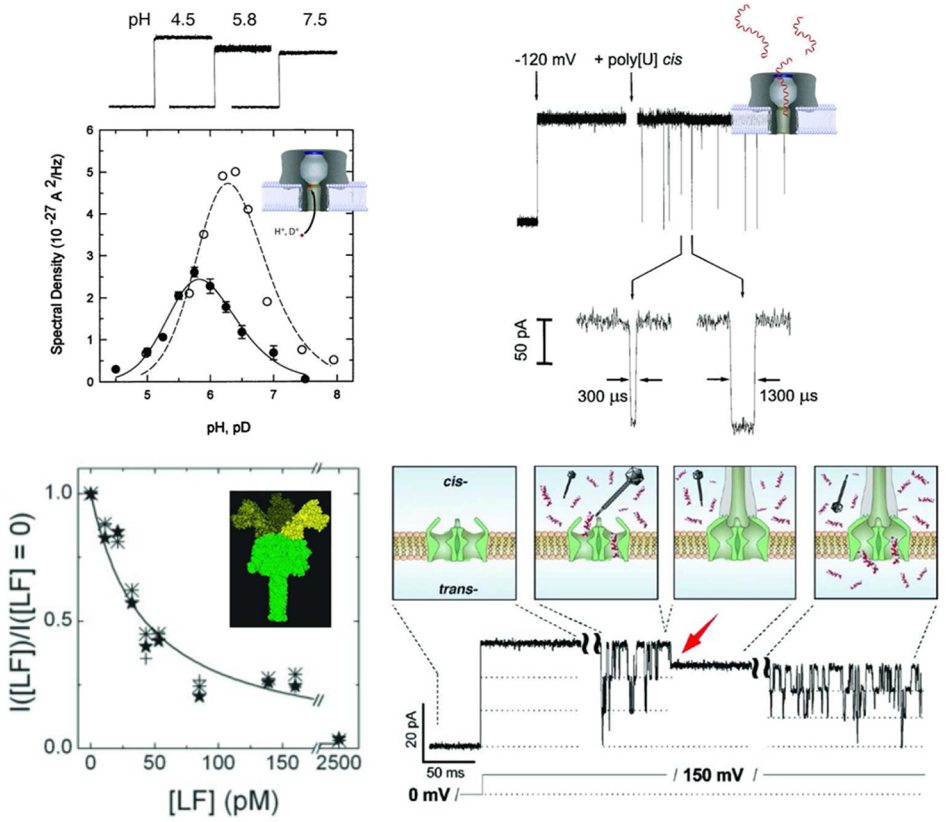

Figure 4. Examples of analytes detected with bacterial pore-forming toxins. Hydronium or deuterium ions cause ionic current random telegraph noise due to the reversible binding to the pore walls (perhaps by altering the electric field gradient in the pore) (top left). The concentration of aqueous protons (open circles) or deuterium ions (filled circles) was estimated from their effect on the mean current (e.g., Figure 3, bottom left) or the noise content (inset) of the α-hemolysin channel. The maximum noise occurs when the analyte concentration is approximately equal to the value of the binding constant.[41] Individual molecules of single-stranded RNA and DNA are detected as they are driven through the pore[50] (top right). The presence of anthrax lethal factor can be determined by its ability to bind strongly to the channel formed by *Bacillus anthracis* protective antigen 63 (i.e., PA_{63}) forming the lethal toxin complex and reducing the pore conductance[70](bottom left). Similarly, single virus particles can be detected with ion channels, as was shown for the bacteriophage lambda phage (Lam B)-maltoporin channel-docking reaction (bottom right).[73]

frequency of analyte-induced conductance changes and the mean time the pore is occupied by the analyte. The analyte concentration can be measured directly from the mean channel current (Figure 3, bottom left), assuming the reaction stoichiometry is 1:1 (red). For cooperative reactions, in which more than one analyte is required to alter the pore conductance, the transition of the channel conductance from its unoccupied to occupied values will be sharper (e.g., a 2:1 analyte/channel stoichiometry response curve is shown in blue). For the simple chemical reaction scheme described by eq 2, the residence time distribution is described by a single exponential (Figure 3, bottom right). Other kinds of interactions could result in different residence time distributions.[50,67]

3. ANALYTE DETECTION, IDENTIFICATION, AND CHARACTERIZATION WITH PROTEIN ION CHANNELS

3.1. Ions

The ability to use a single channel as an analytical sensor,[69] and to discriminate between subtly different ions,[41] was demonstrated in the early 1990s, even when the reactions were a bit too fast (and perhaps too numerous because of the relatively great number of binding sites in the pore) to measure discrete changes in the conductance caused by the analytes. Figure 4 (top left) shows that a single α-hemolysin channel is altered by a change in the solution pH in two ways. The current recordings show that, with an increase in $[H^+]$, the mean current increases monotonically and the current noise increases as the concentration approaches the value of the binding constant and then decreases as the concentration is increased (inset).

Note that the low-frequency current spectral density plot for aqueous protons (filled circles) and deuterium ions (open circles) binding to the channel are doubly valued with respect to the analyte concentration. Thus, to unambiguously determine the concentration of either analyte, one would need to add more of the same analyte, or remove some of the analyte by adding some fresh buffer. If the current noise decreases or increases, then measured concentration corresponds to the value to the left or right of the peak, respectively.

The mean current (not shown) and the low frequency current spectral density (Figure 4, top left) caused by the binding of aqueous protons or deuterium ions overlap. Thus, the two species cannot be distinguished from each other solely from this data. However, because the reaction rate constants are different, the reaction kinetics, and the frequency dependence of current noise (not shown), provides the ability to discriminate between the two isotopes over a limited concentration range.[41]

dx.doi.org/10.1021/cr300381m | *Chem. Rev.* 2012, 112, 6431–6451

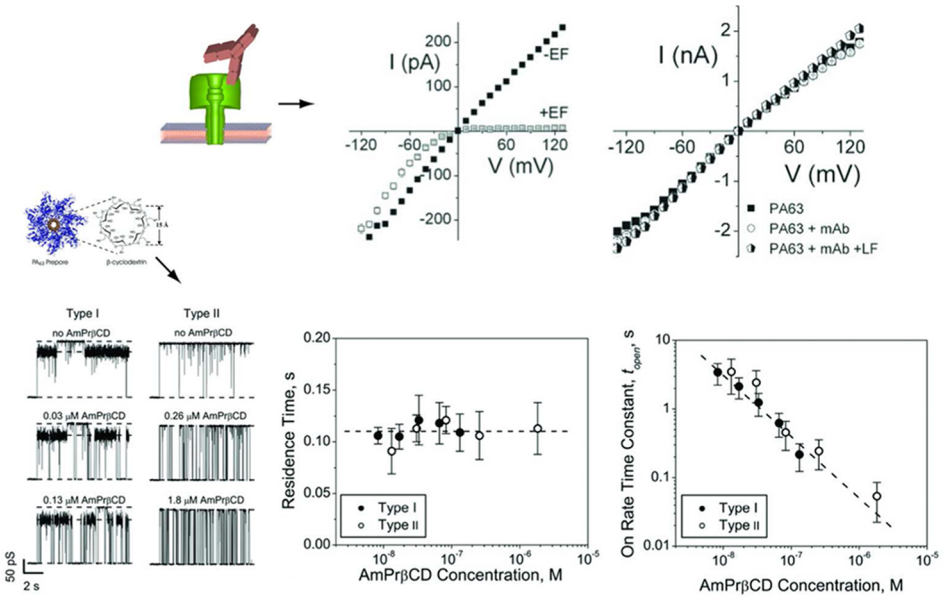

Figure 5. Use of ion channels for the rapid screening of therapeutic agents. Antibodies block the binding site for both *lethal factor* (LF) and *edema factor* (EF). When EF or LF binds to the PA_{63} channel, the ionic current−voltage curve is converted from being nearly ohmic to highly rectifying[70,74] (top middle). When the PA_{63} channel is first treated with a PA_{63}-specific antibody, the binding reaction is blocked (top right). β-Cyclodextrin, modified to maximize the interaction time with the vestibule of the PA_{63} channel, blocks a binding site for the anthrax toxins inside the pore[77] (bottom). Both of these binding sites were identified by ESR measurements.[78]

3.2. RNA and DNA Polynucleotides

In addition to being able to keep the α-hemolysin channel open indefinitely, it was also shown that poly(ethylene glycol) molecules could remain inside the same pore for relatively long times[46] (e.g., >100 μs). Thus, in addition to ions,[41] macromolecules could clearly be detected and characterized by single channels.

In 1996, Kasianowicz and colleagues took advantage of these key features and demonstrated that individual molecules of single-stranded RNA and DNA could be detected as they are driven electrophoretically through a single α-hemolysin channel (Figure 4, top right).[50] The residence time distributions were Gaussian, which suggested the interactions between the polymers and the pore were better described by friction[67] than a simple chemical reaction with a single binding constant (eq 2). The mean residence time of RNA polynucleotides increased in proportion to the polymer length, which suggested the molecules threaded completely through the pore. This hypothesis was confirmed by amplifying the translocated DNA with polymerase chain reaction (PCR): single, but not double, stranded DNA was detected on the opposite side of the membrane.

DNA polynucleotides resist entry into the α-hemolysin channel. For example, it takes ca. 60 mV applied potential to inject the polymer into either end of the pore.[52,59] In addition, because DNA favors entry from the vestibule side of this channel,[44] it is likely that the energy barrier to DNA polynucleotides into the pore is entropic. The height of such barriers will likely depend on the type of analyte to be detected.

3.3. Proteins

Ion channels have also been used to detect specific proteins. For example, the binding of either *Bacillus anthracis* lethal factor (LF) or edema factor (EF) reduced the conductance of channels formed by *B. anthracis* protective antigen 63 (PA_{63}), as shown in Figure 4 (bottom left). The reaction appeared to be reversible (not shown), and characterized by a relatively strong 1:1 binding constant, K = 40 pM.[70] This detection capability is possible because the PA_{63} channel binds LF and EF in vivo in order to transport the two toxins across cell membranes.

3.4. Viruses

The maltoporin (Lam B) ion channel binds sugar molecules[60,71] and has the ability to discriminate between different sugar species.[72] In addition, it is the receptor for bacteriophage lambda virus particles. Bezrukov and colleagues took advantage of that channel's properties in order to detect single phage particles docking to the maltoporin,[73] as shown in Figure 4 (bottom right). That system could also be used to monitor the kinetics of phage/receptor complex formation, which could provide additional information about the interactions and a means to modify them.

3.5. Therapeutic Agent Screening

Existing cell-based methods to screen for therapeutic agents are labor and time-intensive. In the future, that task might be performed more rapidly and easily with electronic systems employing ion channels, which will be illustrated by two examples.

As was mentioned above, two anthrax toxins, *B. anthracis* lethal factor (LF) and edema factor (EF), bind to a channel formed by *B. anthracis* PA_{63}. The toxins convert the channel current−voltage (I−V) relationship from nearly ohmic to highly rectifying[70,74] (Figure 5, top middle). However, it was shown that an antibody known to inhibit the interaction of LF with the PA_{63} channel blocks LF's effect on the channel's I−V curve if it is added before LF (Figure 5, top right) or EF (not shown).[70]

Karginov and colleagues demonstrated that β-cyclodextrins, modified to maximize the interaction time with the vestibule of the PA_{63} channel, bind to the channel[75−77] and decrease the pore conductance (Figure 5, bottom). Although antibodies block the external binding sites for LF and EF described above,

dx.doi.org/10.1021/cr300381m | *Chem. Rev.* 2012, 112, 6431−6451

β-cyclodextrins block binding sites for the toxins inside the pore (e.g., the phenylalanine at residue 427). The binding sites were identified by electron spin resonance (ESR) measurements through site-directed mutagenesis of both the PA_{63} pore and the *N*-terminal fragment of LF.[78] Karginov and colleagues also showed that β-cyclodextrins can block channels from *Clostridium botulinum* and *C. perfringens* and, importantly, protect cells from intoxication by the toxins that bind to the channels.[79]

3.6. Single-Molecule Mass Spectrometry

Nonelectrolyte polymers of poly(ethylene glycol), PEG, were used to estimate the size of the limiting pore aperture for several ion channels (see review by Robertson et al.[80] in this volume), including that formed by α-hemolysin.[81−83] Briefly, because PEGs reduce the bulk conductivity, polymers that are small enough should partition into a channel pore and reduce its conductance. The limiting pore aperture was estimated from the polymer that was just sufficiently small to enter the pore.

Recently, it was shown that the reverse is also possible. Specifically, single channels can be used to determine the size of molecules at high resolution.[47] For example, the degree by which PEG molecules reduce the pore conductance is in direct proportion to the polymer size. The results in Figure 6 show

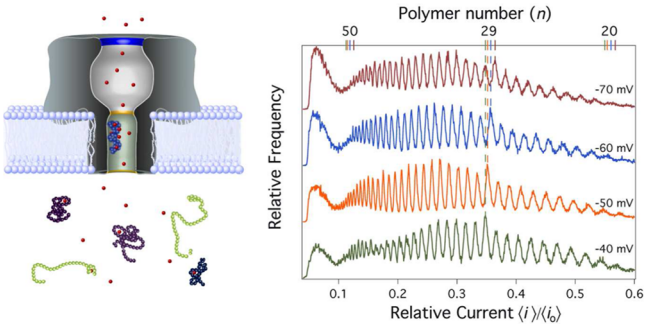

Figure 6. Nanopore-based single-molecule mass spectrometry. The size and charge of single polymers in the α-hemolysin channel can be determined from the degree by which the molecules that enter the pore (multicolored chains, left) reduce the pore conductance via volume exclusion and interactions with ions (red spheres). The method can separate polymers of ethylene glycol at the monomer level (right). Adapted with permission from refs 47 and 49. Copyright 2007 and 2010 National Academy of Sciences.

that the α-hemolysin channel easily separates PEG molecules at the single monomer level (i.e., to better than 44 g mol^{-1}).[47,49] These experiments provided the basis of single-molecule mass spectrometry and demonstrated that a channel can discern small differences between molecules. Knowing the physical and chemical basis of PEG interacting with the α-hemolysin channel allowed the use of PEGs to probe very subtle conformational changes in the ion channel.[84] High-resolution single-channel current recordings in the presence of PEGs demonstrated that the channel's different open states correspond to a simultaneous lengthening and constriction of the α-hemolysin β-barrel of +2.2 Å and −1 $Å^2$, respectively.

In addition to the PEG-induced change in channel conductance, the mean residence times of the polymer in the pore were also markedly affected by the size of the molecule.[47,49] Specifically, the time PEGs spend in the pore increases with polymer size. Thus, the method provides two independent estimates of the polymer size (conductance and mean residence time). The channel conductance and mean residence time can also be used to estimate the number of charges bound to the molecule in the pore. Specifically, a recently developed physical and chemical theory completely accounts for the conductance and residence time as a function of polymer size, charge on the polymer, and applied potential.[49] For reversibly charged polymers (e.g., PEG), the residence-time distribution is exponential, a characteristic of a simple, reversible chemical reaction (such a distribution can present problems for some analytical approaches, which is described later). In contrast, Gaussian residence-time distributions were observed for polymers that have fixed charges on them (such as RNA and DNA polynucleotides)[50] and poly(styrene sulfonate).[48] We believe that the ability to theoretically describe the interactions between analytes and the channel pore[48,67,85−95] will be important for the rational design of nanopore-based sensor technologies.

It should be noted that this single-molecule mass spectrometry method is currently limited to the characterization of relatively small molecules. However, it might be complemented by the recent work of Roukes and colleagues on the development of nanoelectromechanical beams to estimate the mass of single gold nanoparticles (diameters of 5 and 10 nm) and of human IgM proteins.[96]

3.7. DNA Sequencing

As was described above, polynucleotides can be driven, in a rodlike manner, through a single channel (Figure 4, top right). Because single-stranded RNA and DNA thread through the pore, Kasianowicz and colleagues suggested that it might be possible to sequence nucleic acids by reading the ionic current time series like a ticker-tape[50] (Figure 7, far left). That form of nanopore-based DNA sequencing requires that each of the four bases (A,T, G, and C) provides a unique conductance blockade depth or signature. Although homopolymers of cytosine and adenosine cause different degrees of ionic current blockade in the α-hemolysin channel,[51] and diblock copolymers of polyC/polyA show the blockade patterns of the C and A blocks,[51] those results do not provide conclusive evidence for base-by-base sequencing. In fact, although adenosine is larger than cytosine, polyA blocks the channel conductance *less* than does polyC. Because polyC also spends less time in the pore than polyA of the same contour length, it is likely that the α-hemolysin channel is reading multiple bases at a time and is instead reporting the different structures the two homopolymers can adopt. For example, if polyC formed smaller helices than polyA,[97] then it would have a greater number of bases and charge density in the pore than polyA. This *ansatz* is consistent with the experimental results.

Reading DNA in a ticker-tape-like fashion may not be practical because each base is driven through the pore too quickly to be read (ca. 1−10 μs[50,51]). To address that issue, Akeson, Gundlach, and their colleagues are using polymerase to control and reduce the transport rate.[61,99−101] The polymerase binds to a DNA primer and the polynucleotide to be sequenced. The free end of the latter polynucleotide is then driven into the pore, and the complex is held in close opposition to the pore mouth (Figure 7, left). Each cycle of the polymerase adds one base to the nascent duplex DNA outside the pore and concomitantly ratchets the polynucleotide inside the pore by one base. Because ca. 20 nucleotides span the stem region of the α-hemolysin channel,[52,56] it might not be the best channel for sequencing DNA because of the difficulty

dx.doi.org/10.1021/cr300381m | *Chem. Rev.* 2012, 112, 6431−6451

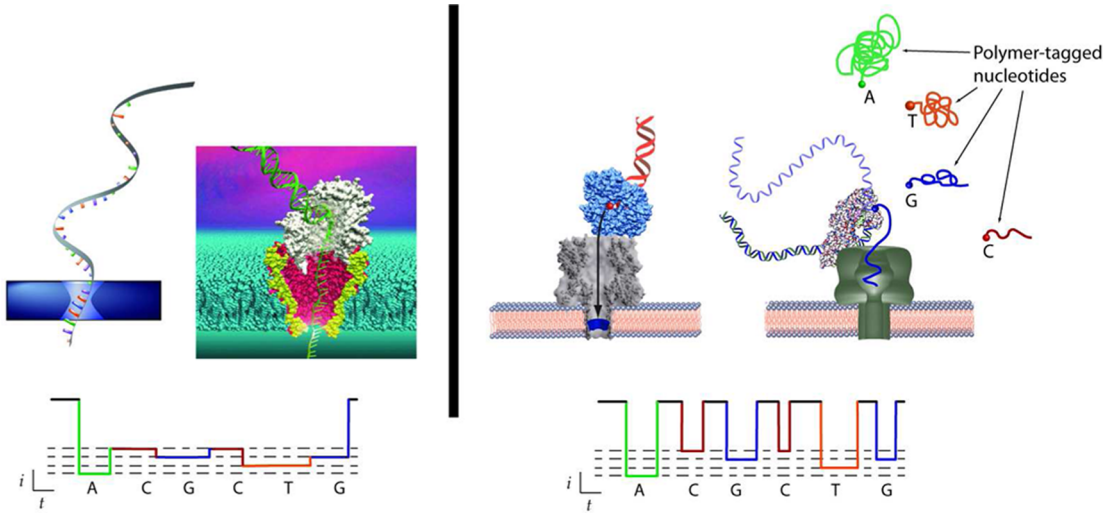

Figure 7. Nanopore-based DNA sequencing engines operate through two possible mechanisms. Reading single-stranded DNA in a ticker-tape fashion[50] by either driving (far left) or pulling (e.g., with polymerase, left) individual polynucleotides through the pore. Left image reprinted with permission from ref 98. Copyright 2012 The American Association for the Advancement of Science. Adapted with permission from ref 61. Copyright 2012 Nature Publishing Group. Assuming that each base causes a unique reduction in channel conductance, and that each base can be held in the detection region of the nanopore long enough to be characterized, this method should be able to sequence extremely long polynucleotides. To overcome the timing limitations of the direct-read me scheme, bases cleaved by exonuclease[105,109]ethods, biochemical processes can produce easier-to-read individual nucleotides or transformations of the nucleotides. In on are to be detected sequentially by a molecular adaptor in a channel (right). In a sequencing-by-synthesis approach, polymer tags that represent the four mononucleotides are released from their respective bases by polymerase and are discriminated by the nanopore (far right).[110]

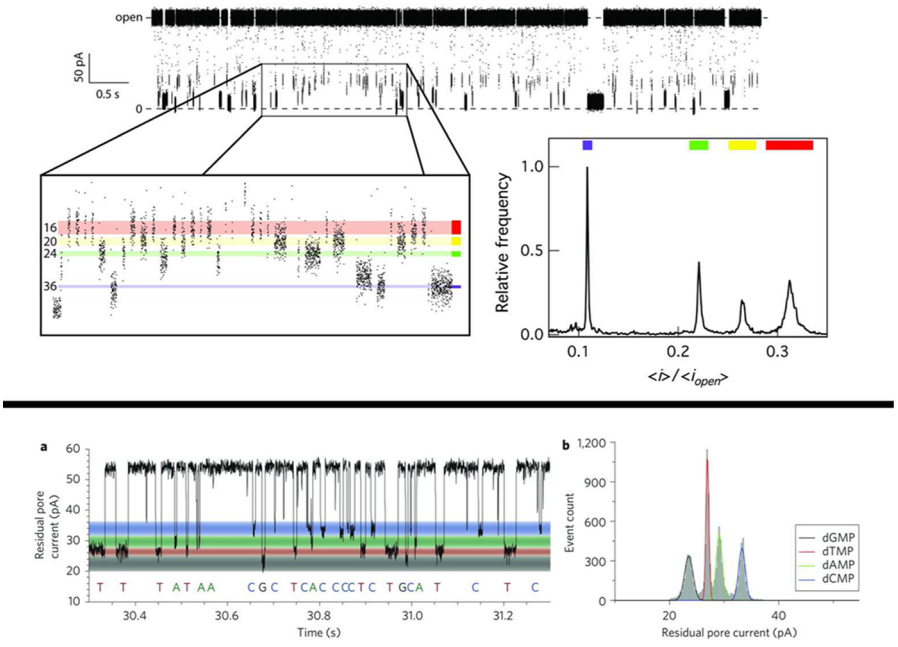

Figure 8. Discrimination of DNA mononucleotides or surrogates with nanopores. The native α-hemolysin channel discriminates between differently sized poly(ethylene glycol) tags representing the four DNA bases to better than one error in 5×10^8 detection events (top). A β-cyclodextrin ring in the α-hemolysin channel separates the four DNA bases with an average accuracy of 92% (bottom). Adapted with permission from ref 109. Copyright 2009 Nature Publishing Group.

determining the contribution of each base to the observed conductance drop.[102] However, the MspA channel, a biological pore derived from *Mycobacterium smegmatis*, may be a better candidate for this application, because the narrowest region of the pore (i.e., the part that will be used to read the DNA bases) is shorter.[61,103,104] Because polymerase runs asynchronously, it is not clear whether this method will be able to identify every base in a homopolymer stretch in a sequence.

Two other methods have been posited for ion channel-based DNA sequencing. One suggested the use of exonuclease attached to the cap domain of the α-hemolysin channel.[105] In this scheme, the enzyme would cleave nucleotides, one at a time, from duplex DNA. Each base would then migrate serially into the pore, bind to a detection/transducer element (e.g., β-cyclodextrin), and be uniquely identified by the degree of ionic current blockade. Because β-cyclodextrin binds mononucleo-

dx.doi.org/10.1021/cr300381m | *Chem. Rev.* 2012, 112, 6431–6451

tides[106−108] and fits well inside the α-hemolysin channel,[109] it was a logical choice for use as DNA base-detection element (Figure 7, right). On the basis of the degree by which the four DNA mononucleotides reduced the conductance of the α-hemolysin channel with a β-cyclodextrin adapter in it, excellent separation of the four bases was achieved.[109] However, there are two fundamental issues with this approach. First, the observed[109] and theoretical capture probability of each cleaved base is too low.[109] Second, the weak binding constants (10 mM < K < 100 mM[106,107]), and the estimated[106,107] and observed mean lifetime of the complexes (i.e., ca. 1 μs[108]), are too short to be of practical use.

DNA and RNA mononucleotides are small, and the differences in their volumes are also small. This presents a significant issue for sequencing with the nucleotide-induced decrease of the channel conductance. To circumvent this problem, Ju and colleagues proposed to use a single channel to discriminate between sequencing-by-synthesis tags (that represent each of the bases) cleaved via polymerase attached to the channel (Figure 7, far right).[110] Figure 8 (top) illustrates proof-of-concept for the ability to separate such tags. Four different size PEGs were well-separated at the 6σ level (1 part in 500 million) with the native α-hemolysin channel, which is substantially better than the separation (ca. 1 part in 10) based on the interaction of mononucleotides with a β-cyclodextrin in the α-hemolysin channel[109] (Figure 8, bottom), which was described earlier. However, it remains to be seen whether polymerase will work when attached to the channel and if the capture rate of the tags is sufficiently great.

Mathe and co-workers study the kinetics of DNA translocation through the α-hemolysin channel using experiments and all-atom molecular dynamics.[111] They found that the direction of DNA translocation affects both the blockade depth of ionic current and the velocity of the molecule. This finding was validated with MD simulations of DNA electrophoretically driven through the pore. These simulations attribute the molecular basis of the directional asymmetry to the difference in the natural tilt angle of the bases, relative to the strand, as they pass the narrowest region of the pore. Further simulation work will be needed to enable the use of nanopores for sequencing applications.

There are other DNA measurement needs beyond sequencing. For example, oxidative and other lesions that damage DNA lead to cancer, heart, and neurological diseases.[112] To improve the ability to detect DNA damage, White and colleagues demonstrated that the α-hemolysin channel can be used to detect abasic segments[113] and other lesions[114] in DNA polynucleotides. It is also possible to modify DNA with chemical labels that add volume to isolated nucleotides in a DNA sequence.[115,116] Although it is not clear if this method will work for sequencing applications, Howorka and colleagues have shown that it is amenable to the detection of single-nucleotide polymophisms by providing a double-stepped resistive pulse when the more massive base translocates the pore.

Many approaches to modifying the α-hemolysin channel involve the addition of cysteine residues in the pore to create reaction sites for the attachment of molecular probes such as PEG[117] or branched polymers such as sulfhydryl-reactive polyamido amine, which alters the chemical and physical nature of the vestibule by filling it with a rigid, positively charged molecular sieve.[118] By preassembling the heptameric pores in rabbit erythrocyte membranes, the PEG-modified pores can be isolated based on the number of cysteine mutants incorporated into the pore. Using this technique, pores can be formed that have anywhere from 1 to 7 identical binding sites with no ambiguity in the number of reaction sites. This technology has been extended to short DNA sequences that can be used to capture complementary sequences.[119]

3.8. Detecting Analytes Larger than the Channel Pore

If a molecule partitions into a channel, and the residence time in the pore is sufficiently long, then the analyte can be detected and characterized. If the molecule is too large to enter the pore, it can still be detected by the pore, but in an indirect manner. For example, instead of adding a recognition site for the analyte inside the pore,[109] the site could be placed on a channel-permeant species.[68] In that manner, the analyte can be detected in one of three ways. First, the capture rate of the unbound pore-permeant species will decrease with an increase in the analyte concentration (Figure 9, left).[68] Second, if the complex

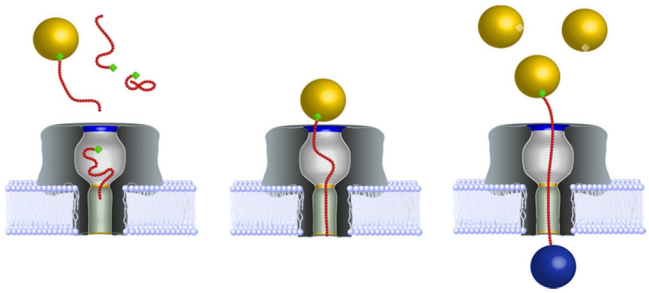

Figure 9. Detecting pore-impermeant analytes with single nanopores.[68] Large analytes (represented by yellow spheres that are too big to enter the pore) can be detected by placing a binding site for them on a smaller molecule that can enter the pore[52,68] (left, middle). Alternatively, a ball-and-chain construct can be used to detect analytes (blue sphere) in an analogy to ice fishing (right).[52,56,68]

can interact with the pore, it will do so and create a different signal than the unbound pore-permeant species (Figure 9, middle). Third, the pore-permeant species could be attached to a large macromolecule that cannot enter the pore, and if it is sufficiently long, the free end of the complex could bind an analyte on the opposite side of the membrane (Figure 9, right). Experimental proof-of-concept for each of these three models was demonstrated over a decade ago.[68]

4. NANOPORE-BASED ANALYSIS OF PROTEINS

In addition to detecting, characterizing, and quantifying a wide range of analytes, ion channels could be used to measure the function and viability of biological molecules. This measurement capability could have far-reaching implications for disease detection and management. As examples, we consider how channels can be used to measure enzyme-turnover rates and study protein folding/unfolding in real time.

4.1. Enzymatic Cleavage

Our understanding of enzyme reactions is derived mostly from ensemble measurements. However, if an enzyme creates products that partition into a channel and react with the channel walls long enough, then the turnover rate of the enzyme can be measured directly, one molecule at a time. For example, ribonuclease A[120] cleaves RNA molecules after pyrimidine nucleotides.[121,122] Kasianowicz and colleagues demonstrated that the α-hemolysin channel could monitor, in real time, the cleavage of RNA polynucleotides.[50] Initially, the

dx.doi.org/10.1021/cr300381m | Chem. Rev. 2012, 112, 6431−6451

polyU homopolymers entered the pore at a rate of about 1 per second (Figure 10, inset top). After adding RNase, the enzyme

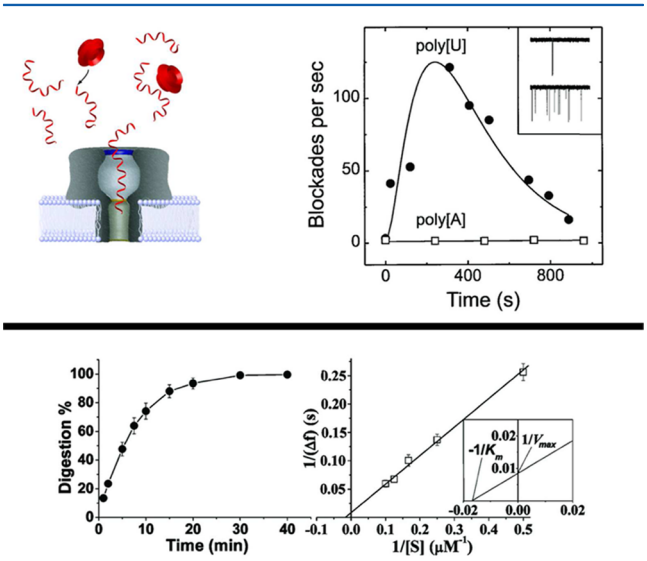

Figure 10. Products of enzyme-catalyzed reactions in the bulk can be detected with a single nanopore (top left). As an example, RNase A cleaves RNA pyrimidines into a larger number of smaller polymers. The initial increase of the polymer concentration caused by the cleavage of 210 nucleotide long polyU is easily detected by a single ion channel (top right, inset and plot). As the reaction progresses, the polyU molecules become so small that the limited bandwidth of the amplifier precludes their detection[50] (top right). The kinetics of trypsin-induced polypeptide digestion monitored with a single ion channel (bottom left). A Lineweaver–Burk plot was used to estimate the Michaelis–Mentin kinetic parameters (K_m and k_{cat}, the dissociation constant for the enzyme–substrate complex and the constant for conversion to product, respectively).[272] Adapted with permission from refs 50 and 123. Copyright 1996 National Academy of Sciences and 2009 American Chemical Society, respectively.

cleaved the polyU into many fragments, which increased the number of RNA polymers that entered the channel per unit time (Figure 10, inset top right). The plot in Figure 10 shows that, initially, the mean capture rate increased, as would be expected if RNase continuously cleaved polyU into random-length polymers. However, eventually, the cleaved polymers became so short that they could not be detected because of the electronic amplifier's limited bandwidth. A control experiment showed that, as expected, RNase did not cleave after purines (e.g., polyA, Figure 10).

More recently, Guan and colleagues demonstrated the use of a single channel to directly monitor the enzymatic cleavage of polypeptides.[123] Specifically, they used a genetically engineered version of the α-hemolysin channel to detect polypeptides cleaved by trypsin (a serine protease that cleaves peptide bonds after Arg or Lys residues[124]). Like RNase A, trypsin is too large to enter the channel pore and, therefore, causes no current blockades by itself. The target short polypeptides caused conductance blockades. After adding trypsin, additional, but newly distinct, current blockades were observed that had shorter mean residence times and blocked the pore conductance to a greater extent. The group was able to follow the reaction to completion and estimate the turnover rate of the enzyme from a Lineweaver–Burk plot. Similarly, a nanopore was used to monitor the enzymatic cleavage of a peptide segment anchored to microscale beads.[125]

4.2. Protein Unfolding via Denaturants and Temperature

The state of a protein's structure (i.e., folded versus unfolded) is typically estimated using optical rotary dispersion (circular dichroism) measurements on protein ensembles.[126–128] These instruments can deduce changes to the protein's secondary and tertiary structure and, therefore, have provided valuable information on protein structure and function.[129–131] They also have aided understanding of the long-standing protein-folding problem.[132–141]

Movileanu and colleagues demonstrated that helical polypeptides can be analyzed directly, one molecule at a time, with the α-hemolysin channel.[142] They engineered barriers on both sides of the β-barrel pore to modify both the entry and exit of these short polymer sequences.[143–145]

Channels are limited to the analysis of small peptides that can easily partition into the pore. Auvray, Mathe, Pelta, and colleagues demonstrated that single channels formed by α-hemolysin, maltoporin, or aerolysin could be used to assess the folded state of individual proteins.[146–149] Folded proteins are too large to enter the channel pore. However, when they are denatured [using either chemicals, e.g., guanidinium chloride[146,147] (Figure 11) or increased temperature[148] (Figure 12)], they can enter the pore and cause blockades in the single-channel current. Plots of the capture frequency as a function of denaturant concentration (Figure 11, bottom) or temperature (Figure 12, bottom) show that the unfolding process occurs over a relatively narrow range of the perturbant, as expected from ensemble measurements with conventional technology.

Other single-molecule techniques (e.g., optical tweezers) were used to study the folding of prions.[150] These methods and the single nanopore-based techniques will hopefully become applicable to the general problem of protein-folding kinetics. As an example, Pelta and colleagues observed how both folded and unfolded proteins interacted with a solid-state analogue of an ion channel.[151] The fabrication and other uses of solid-state nanopores are both discussed in section 6.

5. FORCE SPECTROSCOPY

Defects in biological molecules (e.g., proteins and DNA) often result in debilitating disease. Uncorrected misfolds and aggregation in proteins, especially large multidomain proteins, cause severe diseases such as Parkinson's, Alzheimer's, and cystic fibrosis.[152] On the other hand, defects in DNA replication such as strand slippage[153] and microsatellite instability in DNA replication have been attributed to cause certain cancers including colorectal cancers.[154] There is a need for improved metrology for such defects.

Fluorescence measurements enabled the study of biomolecules in unprecedented detail. Kuzmenkina and co-workers used Förster resonance energy transfer (FRET) to estimate the free -energy landscape from the kinetics of folding and unfolding of proteins.[155,156] Gopich and Szabo developed a theory to model the conformational dynamics of proteins in FRET experiments to provide further refinements to rate constants.[157] Fluorescence experiments can now be supplemented with single-molecule force spectroscopy methods that enable quantifying the interaction forces between biomolecules such as protein side-chains, DNA, and other biological molecules. Nanopore force spectroscopy in conjunction with external techniques such as magnetic tweezers (see refs 158–161), optical trapping, and atomic force microscopy has been used in a wide range of applications. Figure 13 illustrates

dx.doi.org/10.1021/cr300381m | Chem. Rev. 2012, 112, 6431–6451

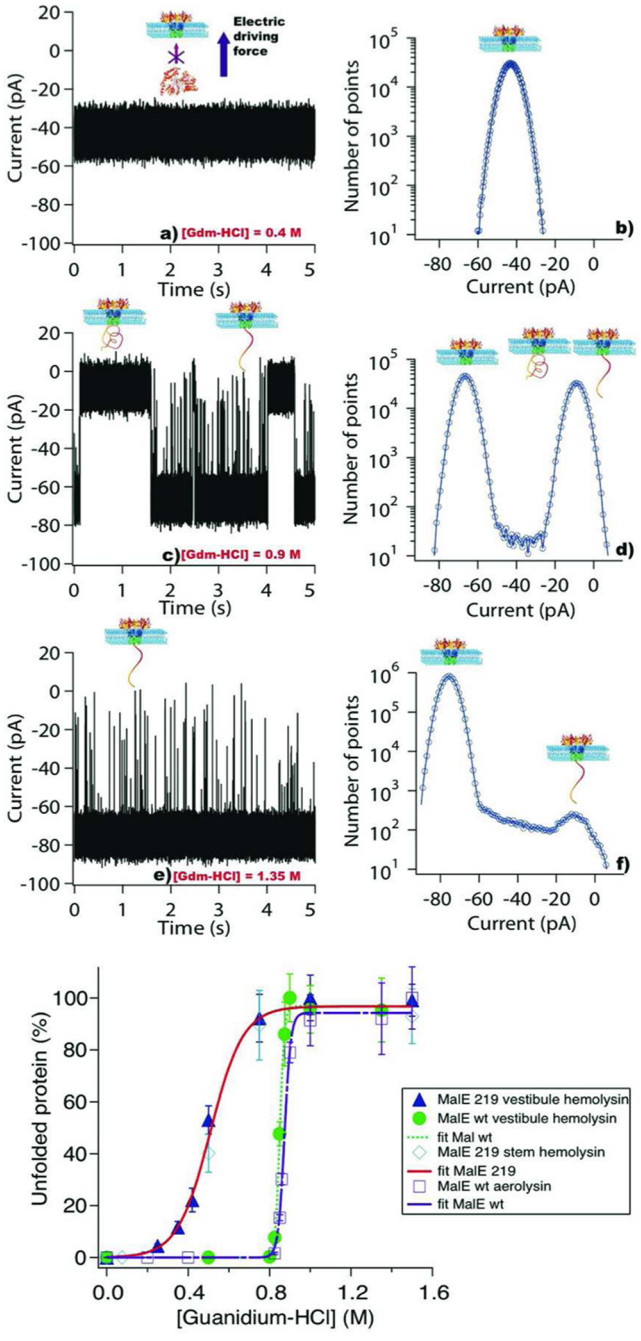

Figure 11. Unfolding of proteins by denaturing agents monitored directly with single channels. At low concentration of the structure perturbant (guanidinium chloride), the folded protein is too large to enter the pore (top left), and the single-channel current is described by single Gaussian (top right). Increasing the concentration of denaturing agent unfolds the protein, which allows the latter to enter the pore and cause current blockades (shown as the additional current level peak, middle two frames). The protein unfolding transition is sharp for proteins interacting with channels formed by aerolysin or maltoporin (bottom). Adapted with permission from ref 149. Copyright 2012 American Chemical Society.

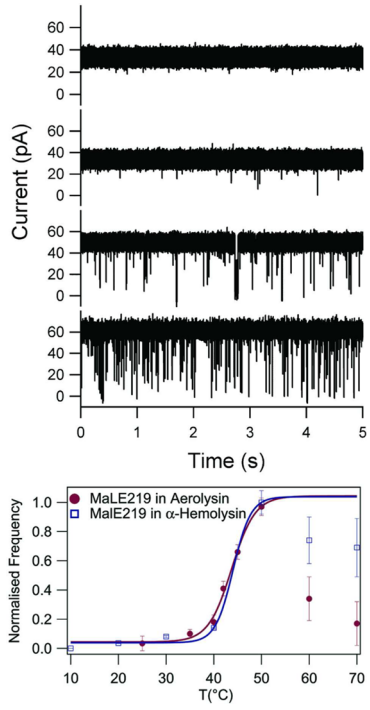

Figure 12. Unfolding of proteins caused by thermal denaturation detected with a single channel. Adapted with permission from ref 148. Copyright 2012 American Chemical Society. Increasing the temperature causes the protein structure to melt, and an applied electric field drives the denatured polypeptides into the pore, one at a time, increasing the current blockade frequency (top). The transition temperature can be estimated from the normalized number of current blockades per unit time (bottom). In this particular experiment, at $T >$ 50 °C, many of the polymer−pore interactions are not detected because the polymers spend too little time in the pore.

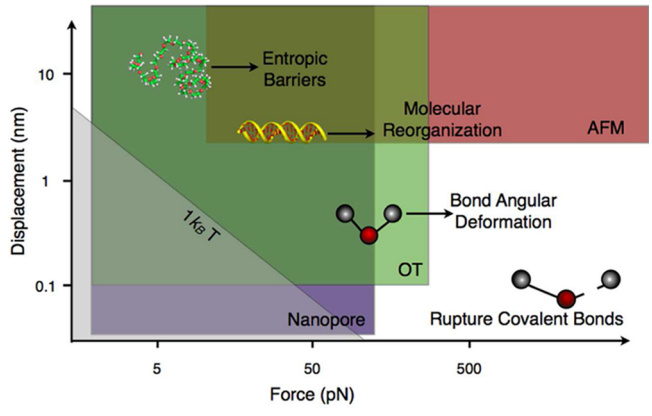

Figure 13. Length and force ranges accessible with single-molecule force spectroscopy. The three colored areas show the applicable force and length scales commonly obtained with AFM, optical trapping, and nanopores. Measurement sensitivity is greatly diminished below the thermal energy of molecules at room temperature shown by the gray shaded region. Although entropic barriers and bond deformations can be probed easily by most methods, AFM measurements are preferred when applying large forces over a long spatial distance. Adapted with permission from ref 273. Copyright 2000 Elsevier.

the applications of these techniques in interrogating biomolecules and the limits of the force applied by each method, which are described in more detail later.

5.1. Nanopore-Based Force Spectroscopy

Nanopores can capture and electrically interrogate single molecules for force spectroscopy applications. By modulating the potential applied across the membrane to control the

dx.doi.org/10.1021/cr300381m | Chem. Rev. 2012, 112, 6431−6451

electrophoretic force acting on the molecule, the rate of capture and translocation can be modified and even reversed.

Kasianowicz and colleagues demonstrated that a polynucleotide attached to a large pore-impermeant macromolecule (i.e., avidin linked to the DNA via biotin) could not traverse the channel.[52,68] Moreover, by reducing the applied potential, the polynucleotide took tens of seconds to back-diffuse out of the channel, which suggested there were significant interactions between the polynucleotide and the pore wall and/or within the polynucleotide.[52] In addition, they suggested that a nanopore could be used to estimate the strength of the interaction between the pore-permeant part of a molecule and another entity bound to it (and, by inference, intramolecular interactions).[68]

The use of an ion channel to estimate the energetics of intramolecular interactions was demonstrated by Akeson and colleagues.[162] They used the α-hemolysin channel to estimate the energy of duplex DNA dissociation in hairpins located at the end of a polynucleotide (Figure 14, top). The free end of the DNA molecule enters the stem region of the pore, and the transmembrane potential exerted a force on the negatively phosphates in the polymer's backbone, which is transmitted directly to the hairpin (Figure 14, top right). Given sufficient time and/or strength of the applied potential, the hairpin can be pulled apart. The mean residence time of the fully structured hairpin in the vestibule correlates with the standard free energy of hairpin formation (Figure 14, bottom). Because energy and force are related, single nanometer-scale pores can readily be used to estimate them on a molecule-by-molecule basis.

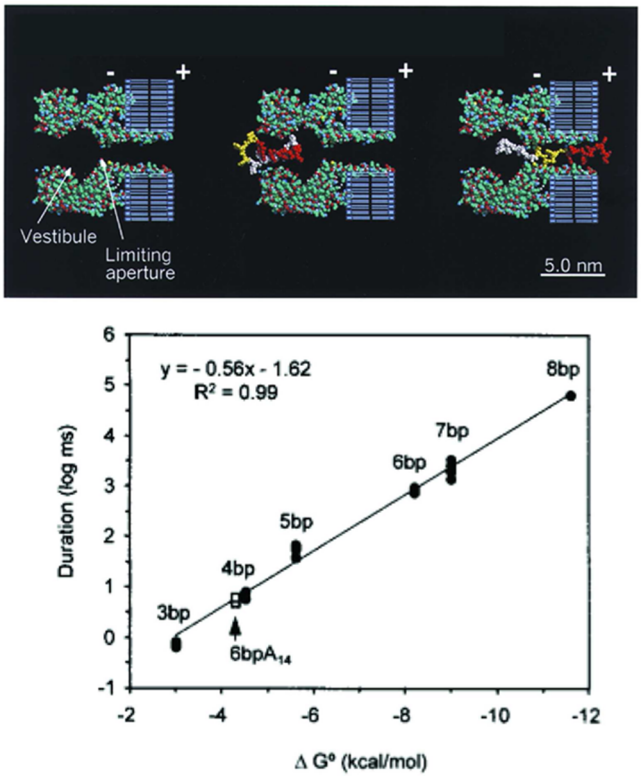

Figure 14. Blockade of the α-hemolysin channel by a DNA hairpin. Cross section of the α-hemolysin channel in the absence of DNA (top left), with a DNA hairpin in the channel vestibule (top middle), and the hairpin pulled apart (top right). The standard free energy of hairpin formation scales linearly with the mean lifetime of an event (bottom). Adapted with permission from ref 162. Copyright 2001 Nature Publishing Group.

The effective electrophoretic force, which balances the bare electrostatic force with the drag force, is given in eq 3, where ε is the dielectric constant of water, R is the radius of the pore, a is the radius of the molecule, $\Phi(a)$ and $\Phi(R)$ are the electrostatic potentials of the pore and molecule, respectively, and ΔV is the potential across the pore.[163,164]

$$F_{el} = \frac{2\pi\varepsilon(\Phi(a) - \Phi(R))}{\ln(R/a)}\Delta V \quad (3)$$

As described above, hairpins formed at one end of single-stranded DNA block the α-hemolysin channel conductance. By applying a linear voltage ramp (thereby increasing the force acting the molecule) until the blockade is cleared, Mathe and colleagues measured the voltage required to unzip DNA hairpins and estimate the effective charge per unit length.[55] A similar technique was used to estimate the mean time required to separate double-stranded DNA with a single-stranded overhang threaded into an α-hemolysin channel.[165] As discussed above, channels have also been used to study the unfolding kinetics of proteins and are able to distinguish between completely unfolded and partially unfolded transition states.[149] Single α-hemolysin channels have also been used to study the dissociation of protein single-stranded DNA/poly(A) complexes using the electrophoretic force to separate the molecules.[166,167]

Nanopore-based force spectroscopy methods are easily combined with other force spectroscopy methods (described below) such as optical trapping. Keyser and co-workers used optical tweezers to apply an external force to stall the translocation of double-stranded DNA through a solid-state nanopore.[163] Spiering and colleagues used optical tweezers to control the translocation rate of a double-stranded DNA–protein complex through a solid-state nanopore and measure force-displacement curves as the complex passes through the nanopore.[168]

5.2. Atomic Force Microscopy

Since its invention, atomic force microscopy (AFM)[169] has been adapted for use in single-molecule methods. AFM is primarily an atomic resolution imaging technique and has been used extensively to study biological molecules in their native state, such as soluble proteins and protein–DNA complexes.[170]

AFM also allows sensitive force spectroscopy experiments with single molecules. These methods are particularly relevant to understanding the nature of misfolds in proteins, which can have catastrophic consequences to human health. Protein unfolding experiments were performed by Carrion-Vazquez and colleagues on an engineered protein made from direct tandem repeat units of the immunoglobin.[171] AFM experiments have since been used to study several systems including the mechanical properties of polypeptides,[172,173] multidomain proteins,[174] ligand–metal reactions,[175] protein–ligand interactions,[176] and, more recently, rate constants of disulfide bonds in polypeptide sequences.[177] In addition to interrogating proteins, AFMs are also used to study the binding of complementary DNA strands[178,179] and antibody–antigen reactions.[180]

AFM pulling experiments are analogous to denaturing experiments where the denaturant is an externally applied force. The additional advantage of this technique in the study of protein folding is that we can explore areas of the energy

dx.doi.org/10.1021/cr300381m | Chem. Rev. 2012, 112, 6431–6451

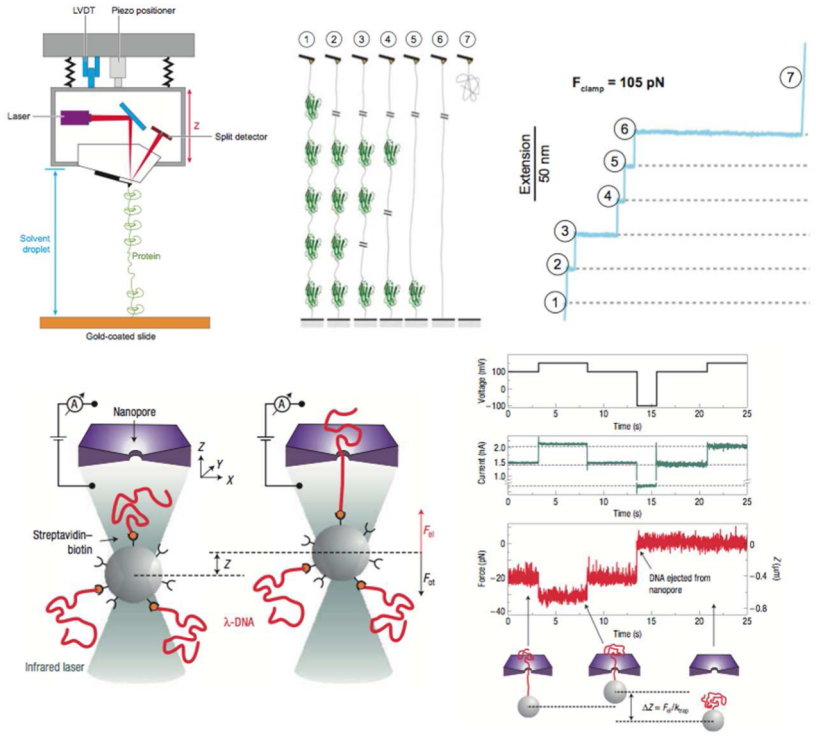

Figure 15. Intermolecular interactions using single-molecule force spectroscopy. An AFM tip can be attached to a single protein and sequentially unwind the secondary structure as in the unfolding of the immunoglobin Ig27 domain (top). Adapted with permission from ref 274. Copyright 2007 Institute of Physics Publishing. Single molecules can also be probed with a nanopore and optical tweezers.[163] DNA attached to a polymer bead can be reversibly threaded into a pore and extended by pulling from both ends, with electric fields inside the pore and in opposition with the optical trap[163] (bottom). Adapted with permission from ref 163. Copyright 2006 American Institute of Physics.

landscape that are not otherwise easily accessible.[181] AFM experiments are run in contact mode as shown in Figure 15, where a silicon nitride cantilever is directly attached to a protein and the protein is completely submerged in solvent.[181] Pulling experiments are run in one of two ways: (i) a constant-velocity measurement where the tip moves at a predetermined constant velocity and the interaction force is recorded or (ii) force-clamp mode where the position of the tip is constantly adjusted to maintain a set force. Results from a force-extension experiment are shown in Figure 15B for a constant-velocity pulling experiment. The sawtooth pattern in the force plot is characteristic of unfolding domains in the protein.

5.3. Optical Trapping

The ability of single beam gradient optical traps[182,183] to perform noninvasive manipulation of micrometer-sized particles, organelles inside biological cells, and even entire biological cells makes them invaluable for use in biophysics experiments.[170] In their most basic form, optical traps provide the ability to manipulate particles in fluids. However, when combined with a sensitive detection system, optical tweezers form a powerful tool to precisely measure and meter the force exerted on a specimen.[184] This ability of optical traps has facilitated their use in the careful characterization of molecular motors such as kinesin,[185] the DNA packaging phi 29 molecular motor,[186] and RNA polymerases.[187−190] Protein-folding studies using optical tweezers have resulted in mapping the folding and unfolding kinetics of the muscular protein titin.[191]

Optically trapped dielectric probes such as silica microspheres have been used to measure the stiffness of the cell wall in red blood cells.[192] Optical tweezers have also been used to study the folding and unfolding kinetics of riboswitch aptamers that regulate gene expression in mRNA molecules,[193] and in combination with fluorescence microscope, optical traps have been used to study the relaxation dynamics of double-stranded DNA.[194]

The precise measurement of optical-trapping forces are a key component to their successful application in the biophysics experiments described. Typically, optical-trapping forces are applied indirectly to a biological molecule through attachment of large probes such as silica microspheres, ca. 1−10 μm in diameter (see Figure 15C). The forces exerted on a probe particle can be described using eq 4, where P is the power of the incident beam, c is the speed of light in vacuum, n_m is the refractive index of the surrounding media, and Q is an efficiency factor. The efficiency factor Q can be theoretically calculated for spherical particles using Mie theory after representing the incident beam in a plane wave basis set or measured experimentally.[195−197]

$$F = \frac{n_m P}{c} Q \tag{4}$$

Large silica microspheres are strongly confined close to the center of an optical trap. Therefore, the forces on these particles are measured under a harmonic approximation that treats the optical trap as a linear spring. The force acting on a particle is then given by $F = -kx$, where k is the stiffness of the trap and x is the displacement from the center. The stiffness of the trap is most commonly measured by taking the Fourier transform of the particle motion in a trap and then calculating its magnitude to obtain a power spectral density (PSD). Under the assumption of a particle in an overdamped oscillator, the PSD has a Lorentzian form described by eq 5, where k_B is the

dx.doi.org/10.1021/cr300381m | Chem. Rev. 2012, 112, 6431−6451

Boltzmann's constant, γ is the Stoke's constant for a spherical particle, T is the temperature, and f_c is the corner frequency of the trap, defined as the frequency at which the magnitude of the PSD decreases by 3 dB.[198,199] The stiffness of the trap is then given by $k = 2\pi\gamma f_c$. The trap stiffness for large particles can also be calibrated using other techniques such as the drag force method[200,201] or the equipartition method.[202,203] For small particles, where the harmonic approximation does not hold, the entire force profile of the optical trap can be measured using the step-response method or by leveraging the stochastic motion of a particle in the trap.[204]

$$S(f) = \frac{k_B T}{2\gamma\pi^2(f_c^2 + f^2)} \quad (5)$$

5.4. Analyzing Data from Pulling Experiments

Data from single-molecule pulling experiments are modeled using an extension to Kramers' chemical kinetics and transition theory.[205,206] The unfolding rate of the protein is calculated using the expression in eq 6,[181] where k_0 is the intrinsic rate constant to be determined, x_u is the distance over the transition state, F is the applied force, k_B is Boltzmann's constant, and T is the temperature. An important implication of this expression is that the unfolding rate is not just a function of the height of the transition state but also the unfolding path. The Bell–Evans formalism described above has been since expanded by Dudko and colleagues to include a higher-order curvature term in the intrinsic rate equation to account for bimodal energy barriers as well as wide transition states.[207,208] This has been followed by a unified description of the kinetics in pulling information that yields the location and height of the transition state along with the intrinsic rate constant.[209–

$$k_u(t) = k_0 \exp\left(\frac{F(t)x_u}{k_B T}\right) \quad (6)$$

6. BIOMIMICRY: SOLID-STATE NANOPORE-BASED SENSORS

As was described earlier, single-protein ionic channels have been used to demonstrate proof-of-concept for detecting, quantifying, and physically characterizing many different types of analytes. However, the ability to adapt them to real-world sensing applications could be limited if they cannot easily be integrated into easily manufactured systems. In an effort to address this potential shortcoming, nanometer-scale pores have been fabricated in several different types of solid-state substrates over the past decade.[43,212,213] We discuss both how these devices are made and their performance relative to protein ionic channels.

6.1. Fabrication of Solid-State Nanopores

Li, Golovchenko, and colleagues' seminal contribution to this nascent field was the development of ion-beam sculpting of an ultrathin silicon nitride membrane.[214–216] Briefly, ions in a tightly focused beam collide with the surface and create a nanoscale crater, which initially results in a ca. 60 nm diameter hole in the support (Figure 16, top left). Interestingly, when the beam is kept on, the atoms in the substrate rearrange (i.e., anneal), such that the pore area shrinks linearly as a function of exposure time at constant beam density. Using this method, holes with diameters of ca. 2 nm were achieved, and the system could detect 500 base-pair-long double-stranded DNA[214]

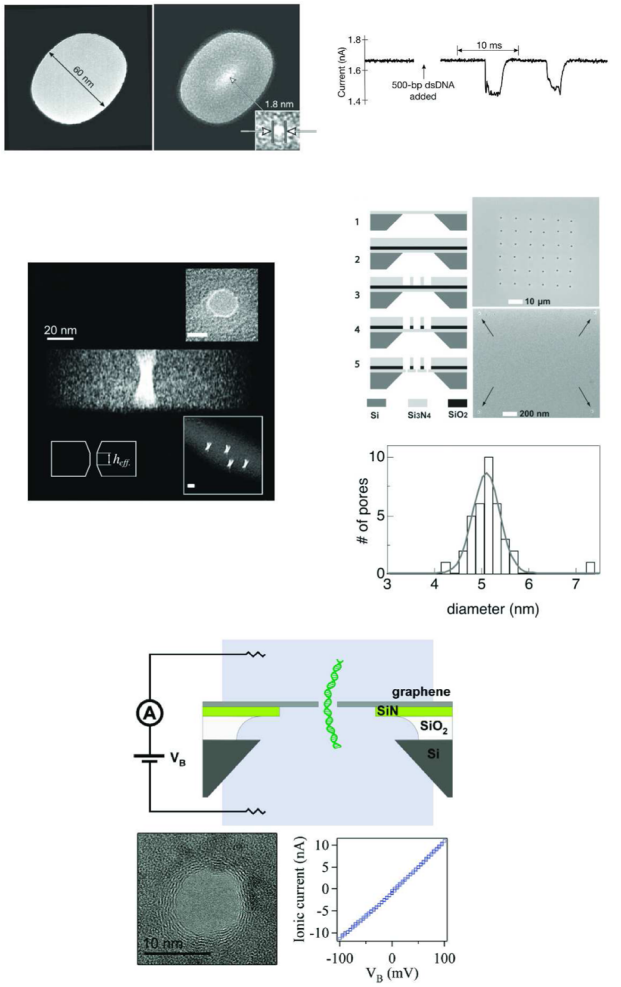

Figure 16. Next-generation nanopores: solid-state varietals. Single pores in silicon nitride ultrathin films[214](top left). Double-stranded DNA (500 bp long) causes ionic current blockades (top right). Geometry of solid-state nanopore determined with transmission electron microscope tomography (middle left). Array of nanopores in a solid-state substrate with a mean pore diameter of 5 nm[220](middle right). Single-atom-long nanopore in a graphene monolayer[231–233]. (bottom). Adapted with permission from refs 214, 220, and 231. Copyright 2001 Nature Publishing Group, 2006 Wiley, and 2010 American Chemical Society, respectively.

(Figure 16, top right). Other groups have extended silicon nitride nanopore development.[212,217–222] For example, Kim and colleagues showed that an array of nanopores could be fabricated in a single solid-state substrate[220] (Figure 16, middle left and right), which could prove crucial to the commercial viability of solid-state nanopore technology.

Nanopores have been fabricated in substrates other than silicon nitride. For example, Bashir and colleagues used an electron beam to fabricate single nanopores in Al_2O_3.[223] Although they showed that a 7-nm-diameter pore could detect double-stranded 5 kbp DNA, the mean transport rate of DNA (<1 ms) is too rapid for most applications. In addition, Siwy, White, and others are developing conical, track-etched nanopores in plastic membranes[224–226] or glass pipettes for sensing applications.[227] It remains to be seen if these more easily fabricated structures will prove to be useful in practical applications.

dx.doi.org/10.1021/cr300381m | Chem. Rev. 2012, 112, 6431–6451

6.2. Detecting Individual Molecules with Solid-State Nanopores

Li and colleagues demonstrated that solid-state nanopores in silicon nitride could also detect single-stranded DNA[228,229] and proteins.[230] One of the potential advantages of solid-state nanopores over those made by channels is their ability to withstand harsher conditions. For example, a solution at pH 11.6 aided the transmembrane voltage-induced unzipping of double-stranded DNA.

Many protein ion channels, especially the one formed by α-hemolysin, have pores that span ca. 4 nm in length. Although such a long channel can resolve small differences in size[47,49] and charge[49] between individual molecules, it is not ideally suited to resolving small features in a single linear polymer (e.g., as one would desire for sequencing DNA). With the hope of addressing this issue, groups led by Drndic, Dekker, and Golovchenko fabricated nanometer-scale pores in a graphene substrate[231−233] (Figure 16, bottom). All three studies demonstrated that this system could detect relatively long double-stranded DNA (≥15 kbp). However, it is not yet clear whether graphene is ideally suited to reading individual bases in single-stranded DNA.

6.3. Next-Generation Solid-State Nanopores

Because they lack the precision architecture (i.e., well-defined and repeatable 3-D stoichiometry and dimensions) and the chemical binding inherent to protein ionic channels, solid-state nanopores by themselves are currently less capable of single-molecule identification and characterization. Research into the development of "smarter" solid-state nanopores may improve that outlook. For example, Azzaroni and colleagues showed that chemically etching a track-etched polyethylene terephthalate solid-state nanochannel and adding an adlayer of 4-vinyl pyridine polymer brushes made the pore conductance responsive to changes in pH.[234,235] The same group demonstrated that adding poly *N*-isopropylacrylamide made a track-etched nanopore's conductance sensitive to changes in temperature.[236] In addition, Zandbergen and colleagues used different electron beam conditions and materials (SiN, SiO_2, and hybrids of SiO_2/SiN/SiO_2) to tune the shape of nanopores.[237]

Kowalczyk and colleagues showed that the translocation times of single-stranded and double-stranded DNA in solid-state nanopores are sensitive to the species of cations in the bulk.[238] Translocation times increased with decreasing cation size and were longest in LiCl solutions. MD simulations of these systems reveal that translocation rates are affected by the binding affinity of cations to DNA, with lithium ions binding more strongly than sodium and potassium (the cations do not bind directly to the DNA strand but instead are coordinated by an intermediate hydration shell).

IBM is reportedly developing a sophisticated solid-state nanopore with nanoscale electrodes embedded into the structure[239,240] (Figure 17, top). The goal is to use the local electric field to control the shape of the molecule in the sensing region and the rate it is transported through the pore. Stolovitsky and colleagues at IBM are also developing theories for such nanopore structures.[241,242]

Biological materials have been used to modify solid-state nanopores. For example, DNA was immobilized on a track-etched conical nanopore, and the pore conductance was altered with a change in solution pH due to the swelling and contraction of the DNA chain.[243]

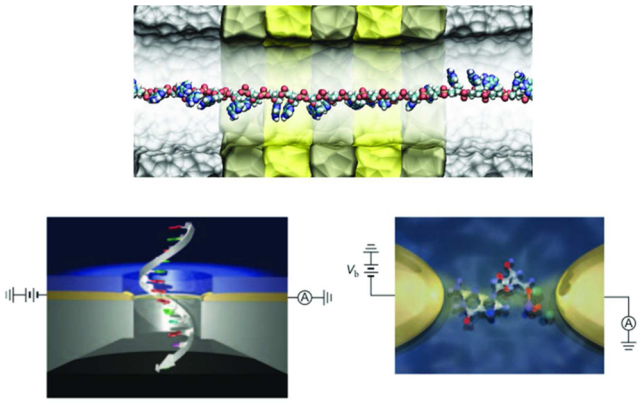

Figure 17. Other conceptual solid-state nanopore-based devices for DNA sequencing introduce additional complexity to control transport and identify the bases. IBM scientists proposed a solid-state nanopore with integrated electrodes, which are used to arrest DNA transport with oscillating electric fields (top). Embedded electrodes or electrode junctions across a nanoconstriction can also be used as the detector elements. Tunneling currents through the bases was suggested as a method to discriminate among each of the DNA bases[248−251]- (bottom). Adapted with permission from ref 251. Copyright 2010 Nature Publishing Group.

Mussi and colleagues attached single-stranded DNA to a silicon nitride nanopore.[244] That process not only reduced the pore diameter but conferred some ability of the pore to detect polynucleotides complementary to those attached to the pore.

In a different approach, single artificial nanopores based on self-assembled DNA "origami" were inserted into 15-nm-diameter solid-state nanopores, and the hybrid structure could detect λ-DNA molecules (48 502 bp) about as well as the unmodified solid-state nanopore.[245] Similarly, DNA orgami pores were fabricated with a free 7-mer sequence overhanging the aperture. When a single-stranded DNA sequence with a complementary sequence enters the pore, the DNA duplex interaction "captures" the target DNA long enough to characterize the target DNA.[246] The potential advantage of the hybrid pores could arise from both a knowledge of the DNA pore architecture and the ability to more easily change the surface chemistry by modifying the DNA.

Wanunu and Meller used two different processes, self-assembly from both bulk solution and under voltage-driven electrolyte flow, to produce chemically coated solid-state nanopores with diameters of ca. 10 and 5 nm, respectively.[247] The adsorbed organosilanes altered the pore conductance and the sensitivity of the pore to bulk solution pH changes.

Instead of sequencing DNA by measuring the base-induced changes in longitudinal ionic conductance, Di Ventra, Zwolak, Kawai, and colleagues suggested that, if two opposing electrodes could be fabricated in a solid-state nanopore, DNA might be sequenced by measuring the transverse tunneling current[248−250] that passes through highest occupied and lowest unoccupied molecular orbital gaps (Figure 17, bottom). Experimentally, Kawai and colleagues showed that they could embed gold electrodes separated by 1 nm in a nanopore but the signals caused by different mononucleotides are heavily overlapped,[251] perhaps because the bases can bind to the gold electrodes, and that the molecular orbital orientation of the same type of mononucleotide may vary significantly with each base.

dx.doi.org/10.1021/cr300381m | *Chem. Rev.* 2012, 112, 6431−6451

Another solid-state system uses two nanopores in series, one in SiN and the other in Si. This device was used to measure the "time of flight" for the transit of single molecules between the two pores. This technology might prove to be useful for a number of applications that require knowledge of the mobility of the target species.[252,253] Mobility measurements were made at relatively low (100 pM) DNA concentration in the presence of a wide range of electrolyte concentrations (e.g., 30 mM < [KCl] < 1 M). The mechanism of DNA transport through the device is elucidated by statistical analysis, showing the free-draining nature of the translocating DNA polymers and a barrier-dominated escape through the second pore. Furthermore, the consecutive threading of single molecules through the two pores can be used to gain more detailed information on the dynamics of the molecules by correlation analysis, which also provides a direct electrical proof for translocation.

Steinem and co-workers demonstrated that channels could be reconstituted into individually addressable lipid bilayers painted on an array of 60-nm-diameter apertures in porous alumina.[254] These nano-bilayer membrane (BLM) structures are somewhat limited for electrical-based single-molecule measurements limitation because the high-aspect ratio of the substrate increases the access resistance, which could confound the use of this technology for single-molecule detection based on electrophysiology measurements. However, that issue could be addressed by making the substrate much thinner.

As was mentioned above, Kim and colleagues demonstrated the ability to make arrays of nanopores in a solid substrate.[220] Rant and co-workers showed that each of the nanopores could be placed over an exceptionally small (30-fL volume) compartment, and that α-hemolysin channels can be reconstituted into each of the membranes formed over the nanopores.[255]

6.4. Modeling Interactions of Analytes and Solid-State Nanopores

Theory and simulation has been used to model the interactions of analytes and biological nanopores (see above) and solid-state varietals.[239,242,256−259] Efforts like these will clearly be needed to rationally design nanopores for specific applications (e.g., force spectroscopy, mass spectrometry, and specific analyte detection).

6.5. Performance of Solid-State Nanopores

Although solid-state pores have potential advantages over ion channels (e.g., mechanical stability), they currently have many disadvantages. First, as was noted earlier, ionic channels have superior control over precise 3-D structure and stoichiometry. In addition, solid-state nanopores exhibit poorer control over noise compared to some ionic channels.[260−264]

Dekker and colleagues showed that the baseline ionic conductance of solid-state nanopores is highly variable and noisy.[261] The authors suggested that the dominant noise source is caused by gaseous bubbles trapped in the solid-state pore. Further studies by that group led them to conclude that Johnson noise predominates at high frequency ($f > 1$ kHz), and the current noise power in the low-frequency regime ($f < 100$ Hz) is inversely proportional to the number of charge carriers (i.e., it is $1/f$ type noise described by Hooge's phenomenological relation: $S/I^2 = \alpha/(N_c f)$ where S is current power spectral density, I is current, α is a parameter, and N_c is the charge carrier number). They used these results to identify the optimal salt concentration for DNA detection. For small pores ($d < 20$ nm), 1 mM electrolyte had a lower signal-to-noise ratio.[263] In addition, Siwy and colleagues showed that, for a conical rectifying pore, $1/f$ noise can be tuned by the applied voltage.[265] Surface charge fluctuations dominate the noise for 0.1 kHz < f < 10 kHz[266] and can be optimized by pH conditions.[264]

Clochard and colleagues studied the noise in single-ion track nanopores in a polyimide film.[267] They demonstrated that the $1/f$ noise amplitude depends on the type of ions in the fluid bathing the nanopore. This implies that the noise is neither the result of fluctuations in pore geometry nor dependent on the surface charge of the pore. Instead, the noise was caused by fluctuations of the liquid conductivity in the pore.

Marziali's group has been developing techniques to reduce noise in solid-state nanopores.[262] To reduce high-frequency noise, they coated the chip with poly(dimethylsiloxane) (PDMS) (Figure 18). This reduced the power spectral density by at least an order of magnitude across the entire frequency range.[262] However, despite the PDMS treatment, the α-hemolysin channel still exhibits significantly less current noise. Conceivably, solid-state nanopore performance might be improved with treatment by oxygen plasma and piranha etching, which presumably improves the hydrophilicity and cleanliness of the surface.

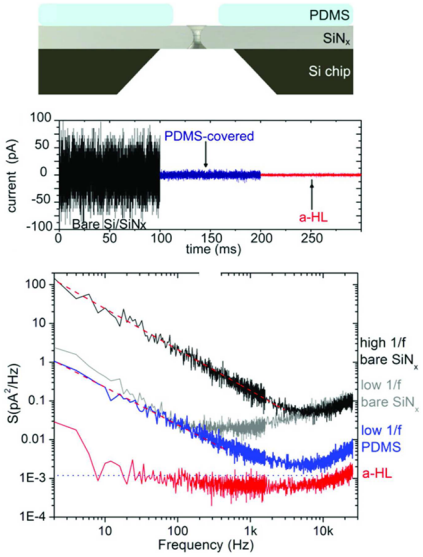

Figure 18. Noise reduction in solid-state nanopores. Ionic current (middle) and current power spectral density (bottom) through a bare silicon/silicon nitride nanopore, a PDMS covered silicon nitride nanopore (top), and the channel formed by α-hemolysin. Adapted with permission from ref 262. Copyright 2007 Institute of Physics Publishing.

An active research area has focused on improvements to solid-state nanopore-based single-molecule sensing. Several groups are modifying the solid-state nanopores first developed by Li et al.[214] Insertion of electrodes directly into the nanopore holds great promise in localizing the sensing field to a volume commensurate with a single nucleotide. Toward this goal, Harrer and colleagues[240] inserted TiN electrodes within a SiO_2 nanopore. They reported problems such as induced surface changes (short-time pore clogging) and intrapore bubble formation. These problems were addressed by passivating the pore surface with an oxide layer through an oxygen plasma treatment and by using a 90% glycerol electrolyte solution. Both of these modifications led to relatively long-term (24 h)

dx.doi.org/10.1021/cr300381m | Chem. Rev. 2012, 112, 6431−6451

nanopore stability. Venkatesan et al. have taken a slightly different approach by hoping to combine the excellent sensing capabilities (specificity and lower noise) of a biological nanopore with the stability of solid-state nanopores. In this work[268] they formed unsupported lipid bilayer membranes on 200-nm holes in an Al_2O_3 surface.

Shepard and colleagues demonstrated that a complementary metal oxide semiconductor (CMOS) preamplifier can be integrated in a chip containing a silicon nitride nanopore.[269] The system performed well, with a signal-to-noise ratio > 5 for a 1-MHz bandwidth. This performance was made possible because of the reduced capacitance on the high-impedance side of the system (i.e., by using an elastomer and placing the headstage close to the pore to reduce stray capacitance of the leads). That system can detect small segments (25 bp) of double-stranded DNA translocating through the nanopore.

One might expect that immersing a dielectric solid-state pore in an ionic solution would be problematic because that would lead to charge instabilities and unexpected flatband transmembrane potential shifts (i.e., fluctuations in the local electrostatic field would cause correlated fluctuations in the ionic current through the pore). Interestingly, single-protein ionic channels (dielectric constant $4 < \varepsilon < 10$) in a lipid membrane ($\varepsilon \approx 2$[270]) are apparently immune to such issues that plague solid-state nanopores. Indeed, as was discussed above, solid-state nanopores exhibit large pore-to-pore variability in conductance as well as current noise.[263] In addition, some solid-state pores work well for days at a neutral pH but exhibit increasing $1/f$ electronic noise, drifting baseline currents, and permanent single-stranded DNA-induced blockages after hours at pH 13.[228] Given the nature by which solid-state nanopores are made, the region bordering the pore is damaged, due to electron-beam or ion-beam sputtering. That region could have many surface states and could be open to mobile ion contamination. Thus, depositing SiO_2 or PDMS could screen this damaged layer and render it less likely to contribute to charge fluctuations. Perhaps the Johnson noise part of the frequency spectrum is shifted to lower or higher frequencies, depending on the surface states (i.e., the noise never actually goes away, it just shifts in frequency).

7. CONCLUSIONS AND PERSPECTIVE

Ion channels have demonstrated a single-molecule measurement capability that could prove useful in systems designed to detect, identify, characterize, and quantify a wide range of molecules. At the very least, these structures, and/or their solid-state equivalents, should eventually prove to be useful for the detection and management of disease.

AUTHOR INFORMATION

Corresponding Author

*E-mail: jereiner@vcu.edu.

Notes

The authors declare no competing financial interest.

Biographies

Dr. Reiner received his Ph.D. in physics in 2003 at the State University of New York at Stony Brook. He joined NIST in 2003 as a National Research Council postdoctoral fellow and continued there until 2011. He is currently an Assistant Professor of Physics at the Virginia Commonwealth University in Richmond, VA. His research interests include single-molecule detection and manipulation with an emphasis on nanopore and optical techniques.

After completing his Ph.D. at the University of Maryland, College Park, Arvind Balijepalli joined NIST in 2011 as a National Research Council postdoctoral fellow. His research interests include single-molecule techniques using nanopores for applications in DNA sequencing. He particularly focuses on using molecular simulations to describe specific interactions of analytes inside nanopores.

Dr. Robertson is a Physical Scientist in the Physical Measurement Laboratory at the National Institute of Standards and Technology (NIST). He received his Ph.D. in chemistry in 2004 from the University of Arizona with Prof. Jeanne Pemberton as an advisor. He

was a postdoctoral fellow with Prof. Wolfgang Knoll at the Max Planck Institute for Polymer Research prior to joining NIST in 2005 as a National Research Council postdoctoral research associate. His primary research interests are in fundamental biophysics, single-molecule biosensing, and advancing measurement science for studying membrane protein structure and function.

Jason P. Campbell received his B.S. and Ph.D. in Engineering Science from the Pennsylvania State University, University Park, PA, in 2001 and 2007, respectively. Since 2007, he has been with the National Institute of Standards and Technology (NIST). He has contributed to more than 50 refereed papers and conference proceedings at national and international conferences. His research interests involve the fundamentals of NBTI, random telegraph noise in highly scaled devices, galvanomagnetic effects, and alternative magnetic resonance measurements.

Dr. Suehle is the leader of and a supervisory electrical engineer in the CMOS Reliability and Advanced Devices Group in the Semiconductor and Dimensional Metrology Division of the Physical Measurement Laboratory (PML) at the National Institute of Standards and Technology (NIST). He received his B.S., M.S., and Ph.D. degrees in electrical engineering from the University of Maryland, College Park, in 1980, 1982, and 1988, respectively. In 1981, he received a Graduate Research Fellowship with the National Institute of Standards and Technology (NIST), Gaithersburg, MD. Since 1982, he has been working in the Semiconductor Electronics Division at NIST, where he is leader of the CMOS and Novel Devices Group. Dr. Suehle's research activities include failure and wear-out mechanisms of semiconductor devices, radiation effects on microelectronic devices, microelectro-mechanical systems (MEMS), and molecular electronic devices. Dr. Suehle has published over 100 technical papers or conference proceedings and holds 5 U.S. patents.

Dr. Kasianowicz is a physical scientist and project leader in the Physical Measurement Laboratory at the National Institute of Standards and Technology (NIST). He earned a B.A. with distinction in Physics from Boston University, a M.A. in Physics, and a Ph.D. in Physiology & Biophysics from SUNY at Stony Brook. His current research interests include ion channel structure–function, single-molecule detection and characterization, and the physics of polymer structure and transport. Dr. Kasianowicz pioneered the use of nanometer-scale pores for DNA sequencing and other analytical applications. Prior to his staff appointments at NIST, Dr. Kasianowicz was an Office of Naval Research post-doctoral fellow at the NIH and a National Academy of Sciences/National Research Council Research Associate at NIST. He is also a Fellow of the American Physical Society.

REFERENCES

(1) Weissmann, G.; Claiborne, R. *Cell membranes: Biochemistry, Cell Biology, & Pathology*; HP Pub. Co: New York, 1975.
(2) McIntosh, T. J.; Waldbillig, R. C.; Robertson, J. D. *Biochim. Biophys. Acta* **1976**, *448*, 15.
(3) Hille, B. *Ion Channels of Excitable Membranes*, 3rd ed.; Sinauer Associates, Inc.: Sunderland, MA, 2001.
(4) Wente, S. R.; Rout, M. P. *Cold Spring Harbor Perspect. Biol.* **2010**, *2*, a000562.
(5) Miller, M.; Park, M. K.; Hanover, J. A. *Physiol. Rev.* **1991**, *71*, 909.
(6) Miller, M. W.; Hanover, J. A. *Cell Biol. Int. Rep.* **1992**, *16*, 791.
(7) Blobel, G.; Dobberstein, B. *J. Cell Biol.* **1975**, *67*, 835.
(8) Blobel, G.; Dobberstein, B. *J. Cell Biol.* **1975**, *67*, 852.
(9) Simon, S. M.; Blobel, G. *Cell* **1991**, *65*, 371.
(10) Simon, S. M.; Blobel, G. *Cell* **1992**, *69*, 677.
(11) Simon, S. M.; Blobel, G. *Subcell. Biochem.* **1993**, *21*, 1.
(12) Agre, P. *Biol. Cell* **1997**, *89*, 255.
(13) Agre, P.; Lee, M. D.; Devidas, S.; Guggino, W. B. *Science* **1997**, *275*, 1490.
(14) Heimlich, G. G.; Bortner, C. D. C.; Cidlowski, J. A. J. *Adv. Exp. Med. Biol.* **2004**, *559*, 189.
(15) Chen, M. M. J.; Sepramaniam, S. S.; Armugam, A. A.; Choy, M. M. S.; Manikandan, J. J.; Melendez, A. J. A.; Jeyaseelan, K. K.; Cheung, N. N. S. *Curr. Neuropharmacol.* **2008**, *6*, 102.
(16) Han, X.; Xi, L.; Wang, H.; Huang, X.; Ma, X.; Han, Z.; Wu, P.; Ma, X.; Lu, Y.; Wang, G.; Zhou, J.; Ma, D. *Biochem. Biophys. Res. Commun.* **2008**, *375*, 205.
(17) Lehen'kyi, V.; Shapovalov, G.; Skryma, R.; Prevarskaya, N. *Am. J. Physiol. Cell. Physiol.* **2011**, *301*, C1281.
(18) Aepfelbacher, M.; Aktories, K.; Just, I. I. 1. *Bacterial Protein Toxins*; Springer: New York, 2000.
(19) Aktories, K.; Just, I. *Bacterial Protein Toxins*; Springer Verlag: Berlin, 2000.
(20) Mourez, M.; Lacy, D.; Cunningham, K.; Legmann, R.; Sellman, B.; Mogridge, J.; Collier, R. J. *Trends Microbiol.* **2002**, *10*, 287.

(21) Blaustein, R.; Koehler, T. M.; Collier, R. J.; Finkelstein, A. *Proc. Natl. Acad. Sci. U. S. A.* **1989**, *86*, 2209.
(22) Manich, M.; Knapp, O.; Gibert, M.; Maier, E.; Jolivet-Reynaud, C.; Geny, B.; Benz, R.; Popoff, M. R. *PLoS One* **2008**, *3*, e3764.
(23) Young, J. A. T.; Collier, R. J. *Annu. Rev. Biochem.* **2007**, *76*, 243.
(24) Cole, K. S.; Curtis, H. J. *J. Gen. Physiol.* **1939**, *22*, 649.
(25) Hodgkin, A.; Huxley, A. *J. Physiol. (London)* **1952**, *117*, 500.
(26) Hodgkin, A.; Huxley, A.; Katz, B. *J. Physiol. (London)* **1952**, *116*, 424.
(27) Katz, B. *Nerve, Muscle, And Synapse*; McGraw-Hill: New York, 1966.
(28) Eccles, J. C. *The Physiology of Nerve Cells*.; Johns Hopkins Press: Baltimore, MD, 1968.
(29) Neher, E.; Stevens, C. F. *Annu. Rev. Biophys. Bioeng.* **1977**, *6*, 345.
(30) Nicholls, J. G.; Martin, A. R. ; Wallace, B. G.; Kuffler, S. W. *From Neuron to Brain: A Cellular and Molecular Approach to the Function of the Nervous System*; Sinauer Associates: Sunderland, MA, 1992.
(31) Doyle, D. A.; Morais Cabral, J.; Pfuetzner, R. A.; Kuo, A.; Gulbis, J. M.; Cohen, S. L.; Chait, B. T.; MacKinnon, R. *Science* **1998**, *280*, 69.
(32) Kandel, E. R.; Schwartz, J. H.; Jessell, T. M. *Principles of Neural Science*; McGraw-Hill: New York, 2000.
(33) Raggenbass, M.; Dreifuss, J. J. *J. Physiol.* **1992**, *457*, 131.
(34) Changeux, J. P.; Kasai, M.; Lee, C. Y. *Proc. Natl. Acad. Sci. U. S. A.* **1970**, *67*, 1241.
(35) Nielsen, K. J.; Watson, M.; Adams, D. J.; Hammarstrom, A. K.; Gage, P. W.; Hill, J. M.; Craik, D. J.; Thomas, L.; Adams, D.; Alewood, P. F.; Lewis, R. J. *J. Biol. Chem.* **2002**, *277*, 27247.
(36) Vincler, M.; Wittenauer, S.; Parker, R.; Ellison, M.; Olivera, B. M.; McIntosh, J. M. *Proc. Natl. Acad. Sci. U. S. A.* **2006**, *103*, 17880.
(37) Zimmerberg, J.; Parsegian, V. A. *Nature* **1986**, *323*, 36.
(38) Rodriguez, B.; Sigg, D.; Bezanilla, F. *J. Gen. Physiol.* **1998**, *112*, 223.
(39) Bezanilla, F. *Physiol. Rev.* **2000**, *80*, 555.
(40) Blaustein, R.; Miller, C. *Nature* **2004**, *427*, 499.
(41) Kasianowicz, J. J.; Bezrukov, S. M. *Biophys. J.* **1995**, *69*, 94.
(42) Fussle, R.; Bhakdi, S.; Sziegoleit, A.; Tranumjensen, J.; Kranz, T.; Wellensiek, H. J. *J. Cell Biol.* **1981**, *91*, 83.
(43) Kasianowicz, J. J.; Robertson, J. W. F.; Chan, E. R.; Reiner, J. E.; Stanford, V. M. *Annu. Rev. Anal. Chem.* **2008**, *1*, 737.
(44) Song, L.; Hobaugh, M.; Shustak, C.; Cheley, S.; Bayley, H.; Gouaux, J. *Science* **1996**, *274*, 1859.
(45) Aksimentiev, A.; Schulten, K. *Biophys. J.* **2005**, *88*, 3745.
(46) Bezrukov, S. M.; Vodyanoy, I.; Brutyan, R.; Kasianowicz, J. J. *Macromolecules* **1996**, *29*, 8517.
(47) Robertson, J. W. F.; Rodrigues, C. G.; Stanford, V. M.; Rubinson, K. A.; Krasilnikov, O. V.; Kasianowicz, J. J. *Proc. Natl. Acad. Sci. U. S. A.* **2007**, *104*, 8207.
(48) Murphy, R. J.; Muthukumar, M. *J. Chem. Phys.* **2007**, *126*, 051101.
(49) Reiner, J. E.; Kasianowicz, J. J.; Nablo, B. J.; Robertson, J. W. F. *Proc. Natl. Acad. Sci. U. S. A.* **2010**, *107*, 12080.
(50) Kasianowicz, J. J.; Brandin, E.; Branton, D.; Deamer, D. *Proc. Natl. Acad. Sci. U. S. A.* **1996**, *93*, 13770.
(51) Akeson, M.; Branton, D.; Kasianowicz, J. J.; Brandin, E.; Deamer, D. *Biophys. J.* **1999**, *77*, 3227.
(52) Henrickson, S.; Misakian, M.; Robertson, B.; Kasianowicz, J. J. *Phys. Rev. Lett.* **2000**, *85*, 3057.
(53) Meller, A.; Nivon, L.; Brandin, E.; Golovchenko, J.; Branton, D. *Proc. Natl. Acad. Sci. U. S. A.* **2000**, *97*, 1079.
(54) Meller, A.; Nivon, L.; Branton, D. *Phys. Rev. Lett.* **2001**, *86*, 3435.
(55) Mathe, J.; Visram, H.; Viasnoff, V.; Rabin, Y.; Meller, A. *Biophys. J.* **2004**, *87*, 3205.
(56) Henrickson, S. E.; DiMarzio, E.; Wang, Q.; Stanford, V. M.; Kasianowicz, J. J. *J. Chem. Phys.* **2010**, *132*, 135101.
(57) Muthukumar, M. *J. Chem. Phys.* **2010**, *132*, 195101.
(58) McGillivray, D. J.; Valincius, G.; Heinrich, F.; Robertson, J. W. F.; Vanderah, D. J.; Febo-Ayala, W.; Ignatjev, I.; Losche, M.; Kasianowicz, J. J. *Biophys. J.* **2009**, *96*, 1547.
(59) Ambjornsson, T.; Apell, S.; Konkoli, Z.; DiMarzio, E.; Kasianowicz, J. *J. Chem. Phys.* **2002**, *117*, 4063.
(60) Kullman, L.; Winterhalter, M.; Bezrukov, S. M. *Biophys. J.* **2002**, *82*, 803.
(61) Manrao, E. A.; Derrington, I. M.; Laszlo, A. H.; Langford, K. W.; Hopper, M. K.; Gillgren, N.; Pavlenok, M.; Niederweis, M.; Gundlach, J. H. *Nat. Biotechnol.* **2012**, *30*, 349.
(62) Coulter, W. H. U.S. Patent 2,656,508, 1953.
(63) Deblois, R.; Bean, C. *Rev. Sci. Instrum.* **1970**, *41*, 909.
(64) Graham, M. *J. Assoc. Lab. Autom.* **2003**, *8*, 72.
(65) Bezrukov, S. M.; Vodyanoy, I.; Parsegian, V. *Nature* **1994**, *370*, 279.
(66) Einstein, A. *Ann. Phys. (Berlin)* **1905**, *17*, 549.
(67) Lubensky, D.; Nelson, D. *Biophys. J.* **1999**, *77*, 1824.
(68) Kasianowicz, J.; Henrickson, S.; Weetall, H.; Robertson, B. *Anal. Chem.* **2001**, *73*, 2268.
(69) Bezrukov, S.; Kasianowicz, J. J. *Phys. Rev. Lett.* **1993**, *70*, 2352.
(70) Halverson, K. M.; Panchal, R. G.; Nguyen, T. L.; Gussio, R.; Little, S. F.; Misakian, M.; Bavari, S.; Kasianowicz, J. J. *J. Biol. Chem.* **2005**, *280*, 34056.
(71) Bezrukov, S. M.; Kullman, L.; Winterhalter, M. *FEBS Lett.* **2000**, *476*, 224.
(72) Bacri, L.; Oukhaled, A.; Hémon, E.; Bassafoula, F. B.; Auvray, L.; Daniel, R. *Biochem. Biophys. Res. Commun.* **2011**, *412*, 561.
(73) Gurnev, P. A.; Oppenheim, A.; Winterhalter, M.; Bezrukov, S. M. *J. Mol. Biol.* **2006**, *359*, 1447.
(74) Panchal, R. G.; Halverson, K. M.; Ribot, W.; Lane, D.; Kenny, T.; Abshire, T. G.; Ezzell, J. W.; Hoover, T. A.; Powell, B.; Little, S.; Kasianowicz, J. J.; Bavari, S. *J. Biol. Chem.* **2005**, *280*, 10834.
(75) Karginov, V. A.; Nestorovich, E. M.; Moayeri, M.; Leppla, S. H.; Bezrukov, S. M. *Proc. Natl. Acad. Sci. U. S. A.* **2005**, *102*, 15075.
(76) Karginov, V. A.; Nestorovich, E. M.; Schmidtmann, F.; Robinson, T. M.; Yohannes, A.; Fahmi, N. E.; Bezrukov, S. M.; Hecht, S. M. *Bioorg. Med. Chem.* **2007**, *15*, 5424.
(77) Nestorovich, E. M.; Karginov, V. A.; Berezhkovskii, A. M.; Bezrukov, S. M. *Biophys. J.* **2010**, *99*, 134.
(78) Jennings-Antipov, L. D.; Song, L.; Collier, R. J. *Proc. Natl. Acad. Sci. U. S. A.* **2011**, *108*, 1868.
(79) Nestorovich, E. M.; Karginov, V. A.; Popoff, M. R.; Bezrukov, S. M.; Barth, H. *PLoS One* **2011**, *6*, e23927.
(80) Robertson, J. W. F.; Kasianowicz, J. J.; Banerjee, S. *Chem. Rev.* **2012**, *112*, DOI:10.1021/cr300317z.
(81) Krasilnikov, O. V.; Sabirov, R.; Ternovsky, V.; Merzliak, P.; Muratkhodjaev, J. *FEMS Microbiol. Immunol.* **1992**, *105*, 93.
(82) Krasilnikov, O. V.; Da Cruz, J. B.; Yuldasheva, L. N.; Varanda, W. A.; Nogueira, R. A. *J. Membr. Biol.* **1998**, *161*, 83.
(83) Krasilnikov, O. In *Structure and Dynamics of Confined Polymers*; Kasianowicz, J., Kellermayer, M., Deamer, D., Eds.; Springer: Dordrecht, The Netherlands, 2002; pp 97−130.
(84) Robertson, J. W. F.; Kasianowicz, J. J.; Reiner, J. E. *J. Phys.: Condens. Matter* **2010**, *22*, 454108.
(85) Muthukumar, M. *J. Chem. Phys.* **1999**, *111*, 10371.
(86) Muthukumar, M. *Phys. Rev. Lett.* **2001**, *86*, 3188.
(87) Muthukumar, M. *J. Chem. Phys.* **2003**, *118*, 5174.
(88) Kong, C. Y.; Muthukumar, M. *J. Chem. Phys.* **2004**, *120*, 3460.
(89) Kong, C.; Muthukumar, M. *J. Am. Chem. Soc.* **2005**, *127*, 18252.
(90) Muthukumar, M.; Kong, C. *Proc. Natl. Acad. Sci. U. S. A.* **2006**, *103*, 5273.
(91) Forrey, C.; Muthukumar, M. *J. Chem. Phys.* **2007**, *127*, 015102.
(92) Wong, C. T. A.; Muthukumar, M. *J. Chem. Phys.* **2008**, *128*, 154903.
(93) Wong, C. T. A.; Muthukumar, M. *J. Chem. Phys.* **2010**, *133*, 045101.
(94) Muthukumar, M. *Polymer Translocation*; CRC: Boca Raton, FL, 2011.

(95) Mirigian, S.; Wang, Y.; Muthukumar, M. *J. Chem. Phys.* **2012**, *137*, 064904.
(96) Hanay, M. S.; Kelber, S.; Naik, A. K.; Chi, D.; Hentz, S.; Bullard, E. C.; Colinet, E.; Duraffourg, L.; Roukes, M. L. *Nat. Nanotech.* **2012**, 1.
(97) Saenger, W. *Principles of Nucleic Acid Structure*; Springer Verlag: Berlin, 1984.
(98) Pennisi, E. *Science* **2012**, *336*, 534.
(99) Gyarfas, B.; Olasagasti, F.; Benner, S.; Garalde, D.; Lieberman, K. R.; Akeson, M. *ACS Nano* **2009**, *3*, 1457.
(100) Lieberman, K. R.; Cherf, G. M.; Doody, M. J.; Olasagasti, F.; Kolodji, Y.; Akeson, M. *J. Am. Chem. Soc.* **2010**, *132*, 17961.
(101) Olasagasti, F.; Lieberman, K. R.; Benner, S.; Cherf, G. M.; Dahl, J. M.; Deamer, D. W.; Akeson, M. *Nat. Nanotech.* **2010**, *5*, 798.
(102) Butler, T. Z.; Gundlach, J. H.; Troll, M. *Biophys. J.* **2007**, *93*, 3229.
(103) Butler, T. Z.; Pavlenok, M.; Derrington, I. M.; Niederweis, M.; Gundlach, J. H. *Proc. Natl. Acad. Sci. U. S. A.* **2008**, *105*, 20647.
(104) Manrao, E. A.; Derrington, I. M.; Pavlenok, M.; Niederweis, M.; Gundlach, J. H. *PLoS One* **2011**, *6*, e25723.
(105) Branton, D.; Deamer, D. W.; Marziali, A.; Bayley, H.; Benner, S. A.; Butler, T.; Di Ventra, M.; Garaj, S.; Hibbs, A.; Huang, X.; Jovanovich, S. B.; Krstic, P. S.; Lindsay, S.; Ling, X. S.; Mastrangelo, C. H.; Meller, A.; Oliver, J. S.; Pershin, Y. V.; Ramsey, J. M.; Riehn, R.; Soni, G. V.; Tabard-Cossa, V.; Wanunu, M.; Wiggin, M.; Schloss, J. A. *Nat. Biotechnol.* **2008**, *26*, 1146.
(106) Formoso, C. *Biochem. Biophys. Res. Commun.* **1973**, *50*, 999.
(107) BritzMcKibbin, P.; Chen, D. *J. Chromatogr. A* **1997**, *781*, 23.
(108) Bae, J.-R.; Lee, C. *Bull. Korean Chem. Soc.* **2009**, *30*, 145.
(109) Clarke, J.; Wu, H.-C.; Jayasinghe, L.; Patel, A.; Reid, S.; Bayley, H. *Nat. Nanotech.* **2009**, *4*, 265.
(110) Kumar, S.; Tao, C.; Chien, M.; Hellner, B.; Balijepalli, A.; Robertson, J. W. F.; Li, Z.; Russo, J. J.; Reiner, J. E.; Kasianowicz, J. J.; Ju, J. *Sci. Rep.* **2012**, *2*, 684.
(111) Mathe, J.; Aksimentiev, A.; Nelson, D. R.; Schulten, K.; Meller, A. *Proc. Natl. Acad. Sci. U. S. A.* **2005**, *102*, 12377.
(112) Cooke, M. S.; Olinski, R.; Evans, M. D. *Clin. Chim. Acta* **2006**, *365*, 30.
(113) An, N.; Fleming, A. M.; White, H. S.; Burrows, C. J. *Proc. Natl. Acad. Sci. U. S. A.* **2012**, *109*, 11504.
(114) Schibel, A. E. P.; An, N.; Jin, Q.; Fleming, A. M.; Burrows, C. J.; White, H. S. *J. Am. Chem. Soc.* **2010**, *132*, 17992.
(115) Borsenberger, V.; Mitchell, N.; Howorka, S. *J. Am. Chem. Soc.* **2009**, *131*, 7530.
(116) Borsenberger, V.; Howorka, S. *Nucleic Acids Res.* **2009**, *37*, 1477.
(117) Howorka, S.; Movileanu, L.; Lu, X.; Magnon, M.; Cheley, S.; Braha, O.; Bayley, H. *J. Am. Chem. Soc.* **2000**, *122*, 2411.
(118) Martin, H.; Kinns, H.; Mitchell, N.; Astier, Y.; Madathil, R.; Howorka, S. *J. Am. Chem. Soc.* **2007**, *129*, 9640.
(119) Howorka, S.; Movileanu, L.; Braha, O.; Bayley, H. *Proc. Natl. Acad. Sci. U. S. A.* **2001**, *98*, 12996.
(120) Raines, R. T. *Chem. Rev.* **1998**, *98*, 1045.
(121) Deavin, A.; Mathias, A. P.; Rabin, B. R. *Nature* **1966**, *211*, 252.
(122) Roberts, G. C.; Dennis, E. A.; Meadows, D. H.; Cohen, J. S.; Jardetzky, O. *Proc. Natl. Acad. Sci. U. S. A.* **1969**, *62*, 1151.
(123) Zhao, Q.; de Zoysa, R. S. S.; Wang, D.; Jayawardhana, D. A.; Guan, X. *J. Am. Chem. Soc.* **2009**, *131*, 6324.
(124) Evnin, L. B.; Vásquez, J. R.; Craik, C. S. *Proc. Natl. Acad. Sci. U. S. A.* **1990**, *87*, 6659.
(125) Kukwikila, M.; Howorka, S. *J. Phys.: Condens. Matter* **2010**, *22*, 454103.
(126) Eyring, H.; Liu, H.-C.; Caldwell, D. *Chem. Rev.* **1968**, *68*, 525.
(127) Purdie, N.; Brittain, H. G. *Analytical Applications of Circular Dichroism*; Elsevier Science Limited: Amsterdam, 1994.
(128) Rodger, A.; Nordén, B. *Circular Dichroism and Linear Dichroism*; Oxford University Press: Oxford, U.K., 1997.
(129) Greenfield, N.; Davidson, B.; Fasman, G. D. *Biochemistry* **1967**, *6*, 1630.
(130) Greenfield, N.; Fasman, G. D. *Biochemistry* **1969**, *8*, 4108.
(131) Chen, Y. H.; Yang, J. T.; Martinez, H. M. *Biochemistry* **1972**, *11*, 4120.
(132) Kuntz, I. D. *J. Am. Chem. Soc.* **1972**, *94*, 4009.
(133) Anfinsen, C. B. *Biochem. J.* **1972**, *128*, 737.
(134) Anfinsen, C. B. *Science* **1973**, *181*, 223.
(135) Baldwin, R. L. *Annu. Rev. Biochem.* **1975**, *44*, 453.
(136) Scheiner, S.; Kern, C. W. *Proc. Natl. Acad. Sci. U. S. A.* **1978**, *75*, 2071.
(137) Némethy, G.; Scheraga, H. A. *Proc. Natl. Acad. Sci. U. S. A.* **1979**, *76*, 6050.
(138) Kuwajima, K.; Yamaya, H.; Miwa, S.; Sugai, S.; Nagamura, T. *FEBS Lett.* **1987**, *221*, 115.
(139) Creighton, T. E. *Proc. Natl. Acad. Sci. U. S. A.* **1988**, *85*, 5082.
(140) Vila, J. A.; Ripoll, D. R.; Scheraga, H. A. *Proc. Natl. Acad. Sci. U. S. A.* **2003**, *100*, 14812.
(141) Booth, P. J. *Curr. Opin. Struct. Biol.* **2012**, *22*, 469.
(142) Movileanu, L.; Schmittschmitt, J. J.; Scholtz, M; Bayley, H. *Biophys. J.* **2005**, *89*, 1030.
(143) Bikwemu, R.; Wolfe, A. J.; Xing, X.; Movileanu, L. *J. Phys.: Condens. Matter* **2010**, *22*, 454117.
(144) Mohammad, M. M.; Prakash, S.; Matouschek, A.; Movileanu, L. *J. Am. Chem. Soc.* **2008**, *130*, 4081.
(145) Wolfe, A. J.; Mohammad, M. M.; Cheley, S.; Bayley, H.; Movileanu, L. *J. Am. Chem. Soc.* **2007**, *129*, 14034.
(146) Oukhaled, G.; Mathe, J.; Biance, A.-L.; Bacri, L.; Betton, J.-M.; Lairez, D.; Pelta, J.; Auvray, L. *Phys. Rev. Lett.* **2007**, *98*, 4.
(147) Pastoriza-Gallego, M.; Rabah, L.; Gibrat, G.; Thiebot, B.; van der Goot, F. G.; Auvray, L.; Betton, J.-M.; Pelta, J. *J. Am. Chem. Soc.* **2011**, *133*, 2923.
(148) Payet, L.; Martinho, M.; Pastoriza-Gallego, M.; Betton, J.-M.; Auvray, L.; Pelta, J.; Mathe, J. *Anal. Chem.* **2012**, *84*, 4071.
(149) Merstorf, C.; Cressiot, B.; Pastoriza-Gallego, M.; Oukhaled, A.; Betton, J.-M.; Auvray, L.; Pelta, J. *ACS Chem. Biol.* **2012**, *7*, 652.
(150) Yu, H.; Gupta, A. N.; Liu, X.; Neupane, K.; Brigley, A. M.; Sosova, I.; Woodside, M. T. *Proc. Natl. Acad. Sci. U. S. A.* **2012**, *109*, 11452.
(151) Oukhaled, A.; Cressiot, B.; Bacri, L.; Pastoriza-Gallego, M.; Betton, J.-M.; Bourhis, E.; Jede, R.; Gierak, J.; Auvray, L.; Pelta, J. *ACS Nano* **2011**, *5*, 3628.
(152) Stefani, M. *Biochim. Biophys. Acta* **2004**, *1739*, 5.
(153) Petruska, J.; Hartenstine, M. J.; Goodman, M. F. *J. Biol. Chem.* **1998**, *273*, 5204.
(154) Vilar, E.; Gruber, S. B. *Nat. Rev. Clin. Oncol.* **2010**, *7*, 153.
(155) Kuzmenkina, E. V.; Heyes, C. D.; Nienhaus, G. U. *Proc. Natl. Acad. Sci. U. S. A.* **2005**, *102*, 15471.
(156) Schuler, B.; Eaton, W. A. *Curr. Opin. Struct. Biol.* **2008**, *18*, 16.
(157) Gopich, I. V.; Szabo, A. *J. Phys. Chem. B* **2007**, *111*, 12925.
(158) Strick, T.; Allemand, J. F.; Croquette, V.; Bensimon, D. *Prog. Biophys. Mol. Biol.* **2000**, *74*, 115.
(159) Kokoszka, J. E.; Waymire, K. G.; Levy, S. E.; Sligh, J. E.; Cai, J.; Jones, D. P.; MacGregor, G. R.; Wallace, D. C. *Nature* **2004**, *427*, 461.
(160) Gore, J.; Bryant, Z.; Stone, M. D.; Nöllmann, M.; Cozzarelli, N. R.; Bustamante, C. *Nature* **2006**, *439*, 100.
(161) Fisher, J. K.; Cribb, J.; Desai, K. V.; Vicci, L.; Wilde, B.; Keller, K.; Taylor, R. M.; Haase, J.; Bloom, K.; O'Brien, E. T.; Superfine, R. *Rev. Sci. Instrum.* **2006**, *77*, 023702.
(162) Vercoutere, W.; Winters-Hilt, S.; Olsen, H.; Deamer, D.; Haussler, D.; Akeson, M. *Nat. Biotechnol.* **2001**, *19*, 248.
(163) Keyser, U. F.; van der Does, J.; Dekker, C.; Dekker, N. H. *Rev. Sci. Instrum.* **2006**, *77*, 105105.
(164) van Dorp, S.; Keyser, U. F.; Dekker, N. H.; Dekker, C.; Lemay, S. G. *Nat Phys* **2009**, *5*, 347.
(165) Sauer-Budge, A.; Nyamwanda, J.; Lubensky, D.; Branton, D. *Phys. Rev. Lett.* **2003**, *90*, 238101.
(166) Hornblower, B.; Coombs, A.; Whitaker, R. D.; Kolomeisky, A. B.; Picone, S. J.; Meller, A.; Akeson, M. *Nat. Methods* **2007**, *4*, 315.
(167) Lin, J.; Fabian, M.; Sonenberg, N.; Meller, A. *Biophys. J.* **2012**, *102*, 1427.

(168) Spiering, A.; Getfert, S.; Sischka, A.; Reimann, P.; Anselmetti, D. *Nano Lett.* **2011**, *11*, 2978.
(169) Binnig, G.; Quate, C.; Gerber, C. *Phys. Rev. Lett.* **1986**, *56*, 930.
(170) Neuman, K. C.; Nagy, A. *Nat. Methods* **2008**, *5*, 491.
(171) Carrion-Vazquez, M.; Oberhauser, A. F.; Fowler, S. B.; Marszalek, P. E.; Broedel, S. E.; Clarke, J.; Fernández, J. M. *Proc. Natl. Acad. Sci. U. S. A.* **1999**, *96*, 3694.
(172) Bustanji, Y.; Samori, B. *Angew. Chem., Int. Ed.* **2002**, *41*, 1546.
(173) Brown, A. E. X.; Litvinov, R. I.; Discher, D. E.; Weisel, J. W. *Biophys. J.* **2007**, *92*, L39.
(174) Peng, Q.; Li, H. *J. Am. Chem. Soc.* **2009**, *131*, 13347.
(175) Kersey, F. R.; Yount, W. C.; Craig, S. L. *J. Am. Chem. Soc.* **2006**, *128*, 3886.
(176) Guo, S.; Li, N.; Lad, N.; Ray, C.; Akhremitchev, B. B. *J. Am. Chem. Soc.* **2010**, *132*, 9681.
(177) Liang, J.; Fernandez, J. M. *J. Am. Chem. Soc.* **2011**, *133*, 3528.
(178) Strunz, T.; Oroszlan, K.; Schafer, R.; Guntherodt, H. J. *Proc. Natl. Acad. Sci. U. S. A.* **1999**, *96*, 11277.
(179) Fuhrmann, A.; Getfert, S.; Fu, Q.; Reimann, P.; Lindsay, S.; Ros, R. *Biophys. J.* **2012**, *102*, 2381.
(180) Schwesinger, F.; Ros, R.; Strunz, T.; Anselmetti, D.; Guntherodt, H. J.; Honegger, A.; Jermutus, L.; Tiefenauer, L.; Pluckthun, A. *Proc. Natl. Acad. Sci. U. S. A.* **2000**, *97*, 9972.
(181) Borgia, A.; Williams, P. M.; Clarke, J. *Annu. Rev. Biochem.* **2008**, *77*, 101.
(182) Ashkin, A.; Dziedzic, J. M.; Bjorkholm, J. E.; Chu, S. *Opt. Lett.* **1986**, *11*, 288.
(183) Visscher, K.; Gross, S. P.; Block, S. M. *IEEE J. Sel. Top. Quantum Electron.* **1996**, *2*, 1066.
(184) Lang, M. J.; Fordyce, P. M.; Engh, A. M.; Neuman, K. C.; Block, S. M. *Nat. Methods* **2004**, *1*, 133.
(185) Block, S. M.; Goldstein, L.; Schnapp, B. J. *Nature* **1990**, *348*, 348.
(186) Smith, D. E.; Tans, S. J.; Smith, S. B.; Grimes, S.; Anderson, D. L.; Bustamante, C. *Nature* **2001**, *413*, 748.
(187) Neuman, K. C.; Abbondanzieri, E. A.; Landick, R.; Gelles, J.; Block, S. M. *Cell* **2003**, *115*, 437.
(188) Revyakin, A.; Ebright, R. H.; Strick, T. R. *Proc. Natl. Acad. Sci. U. S. A.* **2004**, *101*, 4776.
(189) Abbondanzieri, E. A.; Greenleaf, W. J.; Shaevitz, J. W.; Landick, R.; Block, S. M. *Nature* **2005**, *438*, 460.
(190) Herbert, K. M.; La Porta, A.; Wong, B. J.; Mooney, R. A.; Neuman, K. C.; Landick, R.; Block, S. M. *Cell* **2006**, *125*, 1083.
(191) Kellermayer, M.; Smith, S. B.; Granzier, H. L.; Bustamante, C. *Science* **1997**, *276*, 1112.
(192) Mills, J. P.; Qie, L.; Dao, M.; Lim, C. T.; Suresh, S. *Mech. Chem. Biosyst.* **2004**, *1*, 169.
(193) Greenleaf, W. J.; Frieda, K. L.; Foster, D. A. N.; Woodside, M. T.; Block, S. M. *Science* **2008**, *319*, 630.
(194) Perkins, T. T.; Quake, S. R.; Smith, D. E.; Chu, S. *Science* **1994**, *264*, 822.
(195) Gouesbet, G.; Maheu, B.; Grehan, G. *J. Opt. Soc. Am. A* **1988**, *5*, 1427.
(196) Nahmias, Y. K.; Odde, D. J. *IEEE J. Quantum Electron.* **2002**, *38*, 131.
(197) Rohrbach, A.; Stelzer, E. H. *J. Opt. Soc. Am. A* **2001**, *18*, 839.
(198) Buosciolo, A.; Pesce, G.; Sasso, A. *Opt. Commun.* **2004**, *230*, 357.
(199) Lang, M. J.; Asbury, C. L.; Shaevitz, J. W.; Block, S. M. *Biophys. J.* **2002**, *83*, 491.
(200) Sato, S.; Ohyumi, M.; Shibata, H.; Inaba, H.; Ogawa, Y. *Opt. Lett.* **1991**, *16*, 282.
(201) Ghislain, L. P.; Switz, N. A.; Webb, W. W. *Rev. Sci. Instrum.* **1994**, *65*, 2762.
(202) Neuman, K. C.; Block, S. M. *Rev. Sci. Instrum.* **2004**, *75*, 2787.
(203) Florin, E. L.; Pralle, A.; Stelzer, E.; Horber. *J. Appl. Phys. A* **1998**, *66*, S75.
(204) Balijepalli, A.; Gorman, J. J.; LeBrun, T. W.; Gupta, S. K. In *Proc. ASME*, International Design Engineering Technical Conferences & Computers and Information in Engineering Conference, San Diego, CA, 2009
(205) Bell, G. I. *Science* **1978**, *200*, 618.
(206) Evans, E.; Ritchie, K. *Biophys. J.* **1997**, *72*, 1541.
(207) Hummer, G.; Szabo, A. *Biophys. J.* **2003**, *85*, 5.
(208) Schlierf, M.; Rief, M. *Biophys. J.* **2006**, *90*, L33.
(209) Dudko, O. K.; Filippov, A. E.; Klafter, J.; Urbakh, M. *Proc. Natl. Acad. Sci. U. S. A.* **2003**, *100*, 11378.
(210) Dudko, O. K.; Hummer, G.; Szabo, A. *Phys. Rev. Lett.* **2006**, *96*, 108101.
(211) Dudko, O. K.; Graham, T. G. W.; Best, R. B. *Phys. Rev. Lett.* **2011**, *107*, 208301.
(212) Dekker, C. *Nat. Nanotechnol.* **2007**, *2*, 209.
(213) Venkatesan, B. M.; Bashir, R. *Nat. Nanotechnol.* **2011**, *6*, 615.
(214) Li, J.; Stein, D.; McMullan, C.; Branton, D.; Aziz, M.; Golovchenko, J. A. *Nature* **2001**, *412*, 166.
(215) Stein, D.; Li, J.; Golovchenko, J. A. *Phys. Rev. Lett.* **2002**, *89*, 276106.
(216) Li, J.; Gershow, M.; Stein, D.; Brandin, E.; Golovchenko, J. A. *Nat. Mater.* **2003**, *2*, 611.
(217) Storm, A. J.; Chen, J. H.; Ling, X. S.; Zandbergen, H. W.; Dekker, C. *Nat. Mater.* **2003**, *2*, 537.
(218) Storm, A.; Storm, C.; Chen, J.; Zandbergen, H.; Joanny, J.; Dekker, C. *Nano Lett.* **2005**, *5*, 1193.
(219) Storm, A. J.; Chen, J. H.; Zandbergen, H. W.; Dekker, C. *Phys. Rev. E* **2005**, *71*, 051903.
(220) Kim, M. J.; Wanunu, M.; Bell, D. C.; Meller, A. *Adv. Mater.* **2006**, *18*, 3149.
(221) Dimitrov, V.; Mirsaidov, U.; Wang, D.; Sorsch, T.; Mansfield, W.; Miner, J.; Klemens, F.; Cirelli, R.; Yemenicioglu, S.; Timp, G. *Nanotechnology* **2010**, *21*, 065502.
(222) Ayub, M.; Ivanov, A.; Hong, J.; Kuhn, P.; Instuli, E.; Edel, J. B.; Albrecht, T. *J. Phys.: Condens. Matter* **2010**, *22*, 454128.
(223) Venkatesan, B. M.; Shah, A. B.; Zuo, J. M.; Bashir, R. *Adv. Funct. Mater.* **2010**, *20*, 1266.
(224) Apel, P. Y.; Korchev, Y. E.; Siwy, Z.; Spohr, R.; Yoshida, M. *Nucl. Instrum. Methods, Sect. B* **2001**, *184*, 337.
(225) Siwy, Z. S.; Trofin, L.; Kohli, P.; Baker, L.; Trautmann, C.; Martin, C. *J. Am. Chem. Soc.* **2005**, *127*, 5000.
(226) Howorka, S.; Siwy, Z. *Chem. Soc. Rev.* **2009**, *38*, 2360.
(227) Lan, W.-J.; Holden, D. A.; Zhang, B.; White, H. S. *Anal. Chem.* **2011**, *83*, 3840.
(228) Fologea, D.; Gershow, M.; Ledden, B.; McNabb, D. S.; Golovchenko, J. A.; Li, J. L. *Nano Lett.* **2005**, *5*, 1905.
(229) Fologea, D.; Brandin, E.; Uplinger, J.; Branton, D.; Li, J. *Electrophoresis* **2007**, *28*, 3186.
(230) Fologea, D.; Ledden, B.; McNabb, D. S.; Li, J. *Appl. Phys. Lett.* **2007**, *91*, 053901.
(231) Merchant, C. A.; Healy, K.; Wanunu, M.; Ray, V.; Peterman, N.; Bartel, J.; Fischbein, M. D.; Venta, K.; Luo, Z.; Johnson, A. T. C.; Drndic, M. *Nano Lett.* **2010**, *10*, 2915.
(232) Schneider, G. F.; Kowalczyk, S. W.; Calado, V. E.; Pandraud, G.; Zandbergen, H. W.; Vandersypen, L. M. K.; Dekker, C. *Nano Lett.* **2010**, *10*, 3163.
(233) Garaj, S.; Hubbard, W.; Reina, A.; Kong, J.; Branton, D.; Golovchenko, J. A. *Nature* **2010**, *467*, 190.
(234) Yameen, B.; Ali, M.; Neumann, R.; Ensinger, W.; Knoll, W.; Azzaroni, O. *Nano Lett.* **2009**, *9*, 2788.
(235) Yameen, B.; Ali, M.; Neumann, R.; Ensinger, W.; Knoll, W.; Azzaroni, O. *J. Am. Chem. Soc.* **2009**, *131*, 2070.
(236) Yameen, B.; Ali, M.; Neumann, R.; Ensinger, W.; Knoll, W.; Azzaroni, O. *Small* **2009**, *5*, 1287.
(237) Wu, M.-Y.; Smeets, R. M. M.; Zandbergen, M.; Ziese, U.; Krapf, D.; Batson, P. E.; Dekker, N. H.; Dekker, C.; Zandbergen, H. W. *Nano Lett.* **2009**, *9*, 479.
(238) Kowalczyk, S. W.; Wells, D. B.; Aksimentiev, A.; Dekker, C. *Nano Lett.* **2012**, *12*, 1038.
(239) Polonsky, S.; Rossnagel, S.; Stolovitzky, G. *Appl. Phys. Lett.* **2007**, *91*, 153103.

(240) Harrer, S.; Waggoner, P. S.; Luan, B.; Afzali-Ardakani, A.; Goldfarb, D. L.; Peng, H.; Martyna, G.; Rossnagel, S. M.; Stolovitzky, G. A. *Nanotechnology* **2011**, *22*, 275304.
(241) Luan, B.; Afzali, A.; Harrer, S.; Peng, H.; Waggoner, P.; Polonsky, S.; Stolovitzky, G.; Martyna, G. *J. Phys. Chem. B* **2010**, *114*, 17172.
(242) Luan, B.; Peng, H.; Polonsky, S.; Rossnagel, S.; Stolovitzky, G.; Martyna, G. *Phys. Rev. Lett.* **2010**, *104*, 238103.
(243) Xia, F.; Guo, W.; Mao, Y.; Hou, X.; Xue, J.; Xia, H.; Wang, L.; Song, Y.; Ji, H.; Ouyang, Q.; Wang, Y.; Jiang, L. *J. Am. Chem. Soc.* **2008**, *130*, 8345.
(244) Mussi, V.; Fanzio, P.; Repetto, L.; Firpo, G.; Stigliani, S.; Tonini, G. P.; Valbusa, U. *Biosens. Bioelectron.* **2011**, *29*, 125.
(245) Bell, N. A. W.; Engst, C. R.; Ablay, M.; Divitini, G.; Ducati, C.; Liedl, T.; Keyser, U. F. *Nano Lett.* **2012**, *12*, 512.
(246) Wei, R.; Martin, T. G.; Rant, U.; Dietz, H. *Angew. Chem., Int. Ed.* **2012**, *51*, 4864.
(247) Wanunu, M.; Meller, A. *Nano Lett.* **2007**, *7*, 1580.
(248) Lagerqvist, J.; Zwolak, M.; Di Ventra, M. *Nano Lett.* **2006**, *6*, 779.
(249) Zwolak, M.; Di Ventra, M. *Rev. Mod. Phys.* **2008**, *80*, 141.
(250) Tsutsui, M.; Taniguchi, M.; Kawai, T. *Nano Lett.* **2009**, *9*, 1659.
(251) Tsutsui, M.; Taniguchi, M.; Yokota, K.; Kawai, T. *Nat. Nanotechnol.* **2010**, *5*, 286.
(252) Langecker, M.; Pedone, D.; Simmel, F. C.; Rant, U. *Nano Lett.* **2011**, *11*, 5002.
(253) Pedone, D.; Langecker, M.; Abstreiter, G.; Rant, U. *Nano Lett.* **2011**, *11*, 1561.
(254) Schmitt, E. K.; Vrouenraets, M.; Steinem, C. *Biophys. J.* **2006**, *91*, 2163.
(255) Kleefen, A.; Pedone, D.; Grunwald, C.; Wei, R.; Firnkes, M.; Abstreiter, G.; Rant, U.; Tampe, R. *Nano Lett.* **2010**, *10*, 5080.
(256) Aksimentiev, A.; Heng, J. B.; Timp, G.; Schulten, K. *Biophys. J.* **2004**, *87*, 2086.
(257) Sigalov, G.; Comer, J.; Timp, G.; Aksimentiev, A. *Nano Lett.* **2008**, *8*, 56.
(258) Luan, B.; Aksimentiev, A. *J. Phys.: Condens. Matter* **2010**, *22*, 454123.
(259) Jubery, T. Z.; Prabhu, A. S.; Kim, M. J.; Dutta, P. *Electrophoresis* **2012**, *33*, 325.
(260) Chen, P.; Mitsui, T.; Farmer, D.; Golovchenko, J.; Gordon, R.; Branton, D. *Nano Lett.* **2004**, *4*, 1333.
(261) Smeets, R.; Keyser, U.; Wu, M.; Dekker, N.; Dekker, C. *Phys. Rev. Lett.* **2006**, *97*, 88101.
(262) Tabard-Cossa, V.; Trivedi, D.; Wiggin, M.; Jetha, N. N.; Marziali, A. *Nanotechnology* **2007**, *18*, 305505.
(263) Smeets, R. M. M.; Keyser, U. F.; Dekker, N. H.; Dekker, C. *Proc. Natl. Acad. Sci. U. S. A.* **2008**, *105*, 417.
(264) Hoogerheide, D. P.; Garaj, S.; Golovchenko, J. A. *Phys. Rev. Lett.* **2009**, *102*, 256804.
(265) Powell, M. R.; Vlassiouk, I.; Martens, C.; Siwy, Z. S. *Phys. Rev. Lett.* **2009**, *103*, 248104.
(266) Smeets, R. M. M.; Dekker, N. H.; Dekker, C. *Nanotechnology* **2009**, *20*, 095501.
(267) Tasserit, C.; Koutsioubas, A.; Lairez, D.; Zalczer, G.; Clochard, M. C. *Phys. Rev. Lett.* **2010**, *105*, 260602.
(268) Venkatesan, B. M.; Polans, J.; Comer, J.; Sridhar, S.; Wendell, D.; Aksimentiev, A.; Bashir, R. *Biomed. Microdevices* **2011**, *13*, 671.
(269) Rosenstein, J. K.; Wanunu, M.; Merchant, C. A.; Drndic, M.; Shepard, K. L. *Nat. Methods* **2012**, *9*, 487.
(270) Dilger, J. P.; McLaughlin, S.; McIntosh, T. J.; Simon, S. A. *Science* **1979**, *206*, 1196.
(271) Sotelo, C. *Nat. Rev. Neurosci.* **2003**, *4*, 71.
(272) Johnson, K. A.; Goody, R. S. *Biochemistry* **2011**, *50*, 8264.
(273) Clausen-Schaumann, H.; Seitz, M.; Krautbauer, R.; Gaub, H. E. *Curr. Opin. Chem. Biol.* **2000**, *4*, 524.
(274) Bippes, C. A.; Janovjak, H.; Kedrov, A.; Muller, D. J. *Nanotechnology* **2007**, *18*, 044022.